DESIGN OF A HIGH-PRESSURE JET-STIRRED REACTOR FACILITY FOR GAS-PHASE CHEMICAL KINETICS

by

JACOB CONNOR DAVIS

(Under the Direction of Brandon Rotavera)

ABSTRACT

A high-pressure jet-stirred reactor (JSR) was designed and fabricated in order to understand and characterize chemical kinetics with respect to gas-phase chemistry relevant to combustion and atmospheric pollution. The JSR is constructed of fused quartz and utilizes four 1-mm diameter mixing jets to induce turbulent mixing and ensure homogeneity inside the 30 cm^3 reaction volume. The spherical reactor was designed to operate at a maximum pressure of 50 atm, maximum temperature of 1200 K, and minimum residence time of 30 ms. The heating elements of the reactor are comprised of four twin-core heating elements vacuum-brazed onto the surface of Inconel cylinders surrounding the reaction volume and a pre-heating region. The pressure vessel containing the reactor is made of 1.75” thick stainless steel. High pressures are achieved by means of pressure-balancing inside and outside the quartz tube. Sonic probe sampling is used to extract and store gaseous samples for tandem absorption spectroscopy and mass spectrometry analysis.

INDEX WORDS: Chemical kinetics, high pressure, gas phase, biofuel

DESIGN OF A HIGH-PRESSURE JET-STIRRED REACTOR FACILITY FOR GAS-PHASE CHEMICAL KINETICS

by

JACOB CONNOR DAVIS

B.S., University of Georgia, 2016

A Thesis Submitted to the Graduate Faculty of The University of Georgia in Partial Fulfillment of the Requirements for the Degree

MASTER OF SCIENCE

ATHENS, GEORGIA

2019

DESIGN OF A HIGH-PRESSURE JET-STIRRED REACTOR FACILITY FOR GAS-PHASE CHEMICAL KINETICS

by

JACOB CONNOR DAVIS

Major Professor:	Brandon Rotavera
Committee:	Rawad Saleh Jim Kastner

Electronic Version Approved:

Suzanne Barbour
Dean of the Graduate School
The University of Georgia
May 2019

DEDICATION

I am dedicating the thesis to my loving parents, Danny and Polly Davis, who have always supported and encouraged me in every aspect of my life. It is impossible to thank you adequately for everything you have done for me over the years. You have instilled traditional values, a love for learning, and a strong work ethic that has allowed me to reach this milestone. I could not have asked for better parents or role-models. Thank you for everything that you have done and everything that you continue to do.

ACKNOWLEDGEMENTS

I would like to thank Dr. Brandon Rotavera for all of the help and insight that was offered over the past two and a half years, as well as being very understanding and patient during my graduate career. He has been an outstanding advisor that not only taught me the ends and outs of combustion science, but also the professionalism, work ethic, and dedication required for a career as an engineer.

I would also like to thank my fellow graduate students; Alanna Koritzke, Matthew Christianson, Anna Donor, and Alex Larsson for their unwavering support in and out of the lab. They have all become good friends that helped keep moods light during times of stress. I wish them all the best in their future studies and I can’t wait to see the impact they will have on the scientific community. My thanks also goes out to undergraduate researchers; Adam Jackson, Caleb Wiff, and Sam Hartness who helped build and test some of the facilitating components.

Lastly, I would like to give a special thank you to my loving girlfriend Savannah Holbrook. She has stood by me through times of stress and indecision, and has provided nothing but unwavering support and encouragement over the past two and a half years. Reaching this milestone would not have been possible without her love and moral support.

TABLE OF CONTENTS

Page

CHAPTER

LIST OF TABLES

Page

LIST OF FIGURES

Page

CHAPTER 1

INTRODUCTION AND BACKGROUND

Transportation is an essential component of both modern and developing societies and at current consumption levels accounts for the majority of petroleum use worldwide. In 2017, petroleum-based hydrocarbons (namely gasoline, diesel, and jet fuel) accounted for more than 90% of total energy in the U.S. transportation sector (Figure 1). Biofuels, such as ethanol and biodiesel, contributed about 5%, and natural gas contributed nearly 3%. Electricity provided less than 1% of total transportation energy and, despite continued investments in battery technologies and other areas, is projected to remain marginal[3]. While essential for transportation, petroleum-based fuels are carbon-intensive and contribute to certain phenomena like climate change. In addition, because petroleum

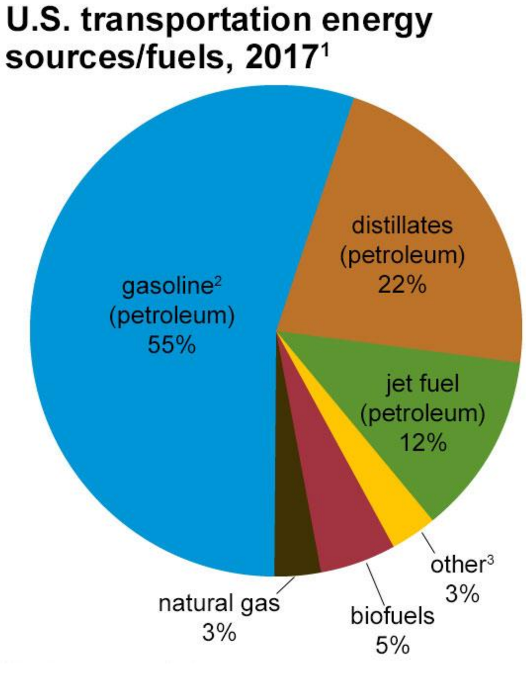

Figure 1: Sources of transportation fuel in the United States in 2017

is a non-renewable resource, energy security and sustainability are inextricably linked to rising consumption levels worldwide.

According to the U.S Energy Information Administration's Annual Energy Outlook 2018, the high energy density of liquid hydrocarbons, in addition to practical matters such as ease of storage and transportability, keep gasoline, diesel, and aviation fuels as the primary energy carriers for transportation for the next several decades at a minimum. While conventional, petroleum-derived hydrocarbons are to remain dominant for the coming decades, research and development efforts for alternative transportation energy are ongoing. As mandated by the Energy Independence and Security Act, biofuels that are of comparatively lower carbon intensity and that can be produced using renewable resources are essential to arriving at a long-term scenario of sustainable transportation energy. Production of such fuels relies on the deconstruction of lignocellulosic biomass. The chemical structure of these biofuels are inherently different than petroleum-based hydrocarbons. Many lignocellulosic-derived biofuels contain functional groups and varying amounts of oxygenation due to the presence of glucopyranose and hemicellulose in the base cellulose molecules[4]. As a result, in order to integrate new biofuels into the transportation sector, fundamental research into the underlying combustion characteristics related to ignition and pollutant formation is needed.

Differences in molecular structure can have a dramatic effect on the combustion characteristics of the fuel, including reactivity, ignition delay time, and energy density. Combustion scientists aim to completely understand how biofuels combust in order to design more-efficient and cleaner-burning engines. To do this, it is imperative to understand how individual biofuels and related fuel blends will react over a wide range of operational conditions including temperature, pressure, equivalence ratio (air to fuel ratio of system compared to air to fuel ratio in an ideal system), and the impact these parameters will have on factors such as energy release, pollution formation, and other environmental aspects. Because of the complex, multi-physics phenomena in practical combustion devices, i.e. heat transfer, fluid dynamics, mass transport, and chemistry, the combustion field is divided into several major overlapping research thrusts.

Combustion chemistry understanding relies on synergy between experimental measurements and computer modeling using chemical kinetics mechanisms, which are designed to predict reactivity, heat release, product formation, and other characteristics at varying pressures, temperatures, and equivalence ratios[5-7]. Chemical kinetics models contain hundreds to thousands of chemical species and consist of rate coefficients for thousands of elementary reactions and are merged with thermochemistry and transport properties of all species included in the model[8, 9]. Engine designers use such mechanisms to develop advanced combustion strategies that maximize the energy output and minimize the production of pollutants that are harmful to human health and to the atmosphere. While chemical modeling and engine design have made significant progress in the past decades, such progress requires the experimental quantification of a wide range of intermediates and products formed during the oxidation process. Combustion experimentalists directly measure reaction intermediates and products that are required to validate the detailed chemical kinetics models. With any computer model, certain reactions must be omitted in order to comply with computational limits given the convergence with Navier-Stokes equations and conservation equations of mass and energy. Data provided by the combustion experimentalist determine which reactions are necessary to include in the model. Gas-phase combustion kinetic studies are traditionally performed using closed vessels, burners, and continuous stirred-tank reactors[1]. These studies aim to record the conversion of the reactants and the mole fractions of reaction products as a function of different parameters such as reaction temperature, residence time, pressure, and composition of inlet gas. The reactivity of the fuel and the selectivity of the reaction products and be deduced from this data.[10] The Jet-Stirred Reactor (JSR) is a state-of-the-art experimental device that, along with advanced diagnostics, provide experimental data needed for fundamental understanding of combustion chemistry.

The motivation to build a high-pressure jet-stirred reactor is to observe and measure species formation that occur during the oxidation of various fuels in temperature and pressure regimes representative of practical combustion devices. The experimental fuel molecules in question are major components of liquid fuels[11] like gasoline or diesel, which are mixtures of various hydrocarbons, or primary intermediates that are formed during the combustion of higher order hydrocarbons[12]. Primary intermediates are stable products that are produced in appreciable concentrations during a combustion reaction of a parent molecule. As mentioned in Koritzke et al.[13] these primary intermediates can have a significant impact on the reactivity of the fuel. For example cyclohexene was discovered to be a primary intermediate of cyclohexane combustion, and displays its own complex chemistry that can impact the reactivity of cyclohexane[13]. Further experimentation is needed to identify and quantify the impact of these primary intermediates.

While the jet-stirred reactor is main experimental device designed in the present work, several other components were also designed and built to support the creation of a complete chemical kinetics experimental facility. These components include: a gas-sample preparation manifold, a flow-control manifold for measurements of absorption cross-sections and electron-impact cross-sections, flow-control manifold for infrared spectroscopy measurements using a Fourier-Transform FT-IR spectrometer, and a gas-compression cell. In addition to the wide range of temperature and pressure achievable by this reactor, multiple analytical techniques were implemented to identify and quantify the reaction products formed during the reaction experiments. The first method of analysis utilizes a Shimadzu IRTracer-100 Fourier Transform Infrared spectrometer (FT-IR) for on-line analysis for time-dependent detection of CO, CO_2, and H_2O formation inside of the reactor. Stabilized IR signals from the FT-IR, as inferred from a plateau in signal level, provide an indication that steady state conditions in the reactor are achieved. Steady state is used to describe the conditions inside the reactor are not changing as a function of time. At this point, gas-phase samples are extracted through a sonic sampling probe and stored for off-line analysis. An Agilent Technologies 7890B Gas Chromatography system (GC) is used to for chromatographic separation of the reaction products. Gas-phase samples are split evenly between two identical columns inside the GC. One column leads to the inlet of the Agilent Technologies 5977B Mass Spectrometric Detector (MS), and the other column leads to the inlet of an electronic absorption spectroscopy diagnostic. The use of two identical columns allows one sample to be simultaneously separated and analyzed using both electron-impact mass spectrometry and electronic absorption spectroscopy. This simultaneous data collection will allow for signal comparison at various retention times, temperatures, and pressures, which enable the determination of reactions mechanisms connecting the observed products. There are many challenges involved with designing a reactor that can conduct experiments at high-pressure, temperature-controlled conditions. Maintaining a homogenous temperature throughout the reaction volume is vital for accurate and repeatable chemical kinetics experiments because of the exponential dependence of reactions on temperature. Many advanced biofuels exhibit dramatic changes in reactivity in the low to intermediate temperature range[14]. Figure 2 shows the oxidation mechanism for low-temperature combustion, occurring ~400 - 1200 K, which is a major topic of interest in combustion research. Figure 2 shows the process for which a fuel (RH) is oxidized by O_2 to produce the combustion products[2]. The first fuel radical (R) is formed via hydrogen abstraction by an OH radical. The fuel radical then reacts with O_2 to form the oxygen centered radical ROO molecule. ROO then self-isomerizes to form a carbon centered QOOH molecule. The reactivity of the fuel depends on the fate of this QOOH molecule. The QOOH can form stable products like conjugate alkenes, cyclic ethers/ carbonyls, and β-scission products plus one radical. Since the total number of radicals is remaining the same these reactions are considered chain propagating reactions, and inhibit the reactivity of the fuel. The second option for the QOOH is to react with O_2 for a second time. As the reaction proceeds in this direction the number of radicals increases from the one QOOH radical to a stable product plus two OH radical. Since there is a net increase in radicals for this pathway these reactions are considered chain branching reactions, and increase the reactivity of the fuel. The trade-off between the chain branching reactions and chain propagating reactions is a function of temperature. The interest in low temperature combustion is because of the inhibiting effect on the formation of harmful pollutants such as NO_x at these temperatures.

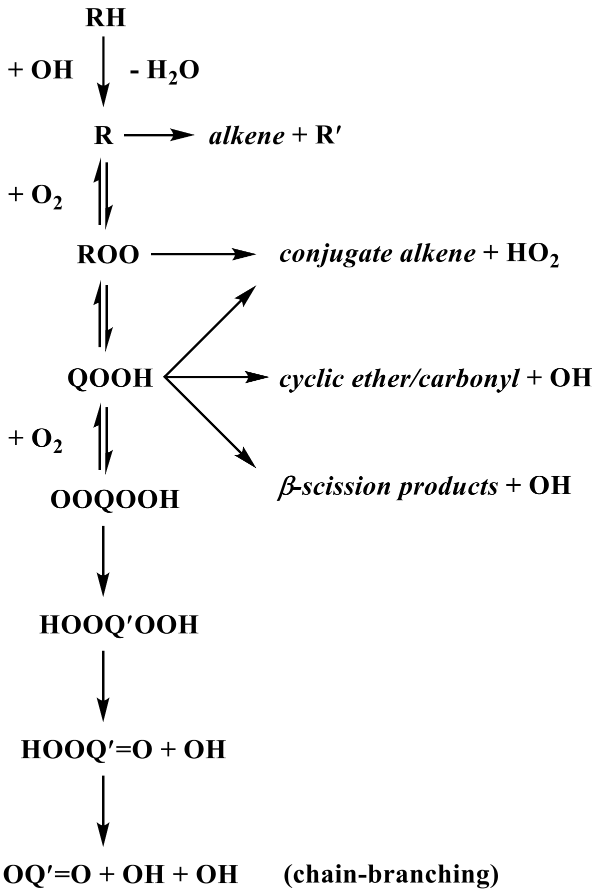

Figure 2: Low-temperature oxidation mechanism of hydrocarbons[2].

David and Matras described the rules of construction for a jet-stirred reactor, detailing the physics of homogenous mixing in the gas phase. However, minimal attention was paid to the homogeneity of the temperature[15]. Understanding and minimizing the thermal gradients present inside the reactor is crucial to accurately collecting data for gas phase kinetics of advanced biofuels[16].

Pressure also has an important effect on the reactivity of most chemical reactions. While understanding the chemical kinetics of various fuels at atmospheric pressure is important, exploring the effects of pressure is essential to be able to fully integrate new biofuels into the transportation sector because practical combustion devices operate at high pressure – 10 atm and higher. Increased pressure increases molecular collision rates and affect rates of the reaction. To investigate the effects of pressure on the reactivity of biofuels and hydrocarbons, the reactor was designed with the capability to perform experiments at pressures that more closely represent the conditions inside of an engine. While low-temperature combustion reduces the amount of pollutants formed, it also reduces the energy released by the combustion reaction because engine efficiency is tied to pressure. To mitigate the drop in energy release, next-generation engine strategies utilize higher in-cylinder compression ratios to maintain or improve power output. Development of high-efficiency engines that can perform at higher compression ratios is an immediate goal of the automotive industry. Operating at high compression ratios is desirable because it allows an engine to extract more mechanical energy per unit mass of fuel.

One type of engine concept designed to capitalize on this principle is the Homogenous Charge Compression Ignition (HCCI)[17] engine. In an HCCI engine, the fuel and air are mixed together either in the intake system or in the cylinder with direct injection. The premixed fuel and air mixture is then compressed. Towards the end of the compression stroke, combustion is initiated by auto-ignition similar to a diesel engine in the sense that combustion is initiated without the presence of a spark plug. The combination of a premixed fuel and air mixture with higher compression ratios will simultaneously reduce fuel consumption and harmful NO_x and particulate emission[17]. Understanding the chemical kinetics of biofuels at these higher pressures and lower temperatures is vital to making these high efficiency engines a reality.

In summary, there is a demand for renewable fuels to be integrated into the transportation sector. Due to the source of the feedstock, the majority of sustainable biofuels contain functional groups or different levels of oxygenation that complicate the combustion chemistry compared to petroleum derived fuels. Low temperature combustion practices are used to limit the amount of harmful pollutants produced by combustion. Experimental data at low temperature and high pressure is needed for these new biofuels in order to develop cleaner burning and more efficient engines.

This paper explains how the concept of a jet-stirred reactor was improved upon to allow for experiments at low temperatures and high pressures. The heating design of previous JSR’s was reengineered to help decrease any thermal gradients near the reaction volume and combat any changes in heating that may arise from human error. Also, a pressure vessel was implemented to utilize pressure balancing across a thin quartz reactor. This pressure balancing extended the experimental range to pressures more closely representative of in-engine conditions.

CHAPTER 2

BACKGROUND OF REACTOR DESIGN

Over time, scientists have developed numerous experiments to study detailed chemical kinetics that takes place during a combustion reaction. Most of these experimental devices can be classified into three main categories; closed vessels, flame burners, and continuous stirred-tank reactors. The jet-stirred reactor falls into the continuous stirred-tank reactor sub-category. Each experiment has advantages and disadvantages and can provide a wide range of various information.

Closed vessel experiments, such as shock tubes and rapid compression machines, are designed to analyze peak pressure, maximum rate of pressure rise, time necessary to reach the peak pressure, the explosion index[18], ignition delay times[19], and chemical kinetics[20]. Flame burners, which can be further categorized into laminar and turbulent flames, are optimized to study flame structure, flame propagation speed, chemical speciation measurements, and reaction kinetics[21]. Because of interest in conducting speciation measurements and analyzing intermediates from low-temperature combustion under controlled conditions of temperature and pressure, a jet-stirred reactor was designed and constructed in the present work for several reasons including:

- Precise control over experimental conditions including temperature, pressure and residence time
- Modeling capabilities using a CSTR fluid flow and chemical kinetics model
- Rapid mixing of gases providing homogenous composition inside the reactor[10].

A continuous stirred tank reactor (CSTR) mentioned above describes a type of steady state reactor that assumes homogenous conditions (temperature, pressure) inside the reaction volume. The jet-stirred reactor at the University of Georgia is designed to conduct chemical kinetics experiments at temperatures ranging from 500 – 1200 K, pressures ranging from 1 – 50 atm, and residence times ranging from 30 ms – 2 s.

Jet-Stirred Flow Reactors

A jet-stirred reactor is a spherical flow reactor with tubular extensions that operates as a continuous flow apparatus and is used to study chemical kinetics. Flow reactors are well-suited for controlling the variables that are most important to chemical kinetics studies including temperature, pressure, and residence time. When operated at steady state and at constant residence time, temperature, and pressure, reactions inside of a JSR are modeled by a system of mass and energy balances coupled to chemical rate equations. Another advantage of a JSR is the ability to couple with analytical techniques such as gas chromatography, mass spectrometry, and VUV spectroscopy for the identification and quantification of species in the gas phase. To promote homogeneity in temperature and species concentration, Jet-stirred reactors induce turbulence primarily in a region above the spherical reactor secondarily by means of four quartz jets (Figure 3). Despite a pressure drop, due to the reaction volume being significantly larger than the volume of the nozzle, in the nozzles, this technique provides very intense internal recycle streams inside the reaction volume[10]. Proper mixing is key to ensuring homogeneous conditions and experimental repeatability.

Figure 3: Four turbulent jets are used to provide secondary mixing inside the spherical reaction volume.

Quartz was used to construct the reactor due to the chemical inertness, which prevents catalytic wall effects from heterogeneous chemistry, and high melting point of the material (1650 °C). Catalytic wall effects refer specifically to unwanted chemical reactions that might occur when the reactants or products come into contact with the walls of the reactor. Such wall reactions could skew the intended results and inhibit the ability to accurately measure the products formed from the target combustion reactions.

The residence time of the gas (Eq. 1) in the reactor is an average time gases spend inside the reaction volume and is a function of the reactor volume, V, and the volume flow rate of the gas flowing through the reactor, $\dot{V}$. Flow-tracer analysis can be used to verify if the reactor can be considered as a continuous stirred-tank reactor, which is conducted by injecting a small amount of tracer in the inlet of the reactor and measuring the concentration of the tracer exiting the reactor as a function of time[1]. If the reactor is an ideal continuous stirred-tank reactor then the residence time distribution $E(t)$ should be represented by Eq. 2.

$$\tau = V/\dot{V} \tag{1}$$

$$E(t) = \frac{1}{\tau} e^{\frac{t}{\tau}} \tag{2}$$

Historical Overview of Jet-Stirred Reactors

Thermal homogeneity is of the utmost importance in gas-phase chemical kinetics as the reaction rates are exponentially dependent on temperature. While proper mixing of the gas inside the reactor took precedence in the construction of the first few jet stirred reactors[16] temperature homogeneity received little attention. In 1979, Azay and Come studied the influence of pre-heating the gas before injection into the reaction volume. Temperature gradients up to 80 K were observed inside their reactor with no preheating[16]. After this discovery, pre-heating sections were affixed to the upstream/inlet side of future reactors. Dilution of the fuel in an inert gas also had dramatic effects on the temperature homogeneity inside the reactor. Due to the exothermicity of combustion reactions, fuel concentrations are kept low, on the order of 10^2 – 10^3 ppm, to limit the effect the heat release has on temperature inside the reaction volume.

In 1986 Dagaut et al. of CNRS- Orléans in France extended the experimental investigation range of their JSR to investigate the effect of pressure on the reactivity of fuels[22] by surrounding the reactor with a stainless-steel pressure jacket that enabled high-pressure experiments by means of pressure balancing inside and outside the reactor. They achieved this by drilling holes in the bottom of their reactor and allowing the exhaust from the reactor to balance the pressure (Figure 5). Pressure control was achieved by means of a pressure regulator downstream of the reactor. This allowed experiments ranging from 1 – 40 atm to be conducted. This design poses a complication because of the potential for the reaction intermediates and products from the reactor to condense on the inside of the pressure vessel This increases the chance of contaminating future experiment, and requires the reactor to be taken apart and cleaned regularly.

Also, in 1986 the team of Dagaut et al. made another change to the design of the JSR. The injectors were shifted towards the upper part of the sphere (Figure 5). Before then, the mixing jets were commonly located in the equatorial plane of the reaction volume (Figure 4), which limits the distance the sonic probe can travel, and therefore limits the sampling area of the reactor. The new design with raised jets allows for an investigation of a larger portion of the reaction volume. By means of a linear motion thimble, which translates the sonic sampling probe, gas samples can be extracted along

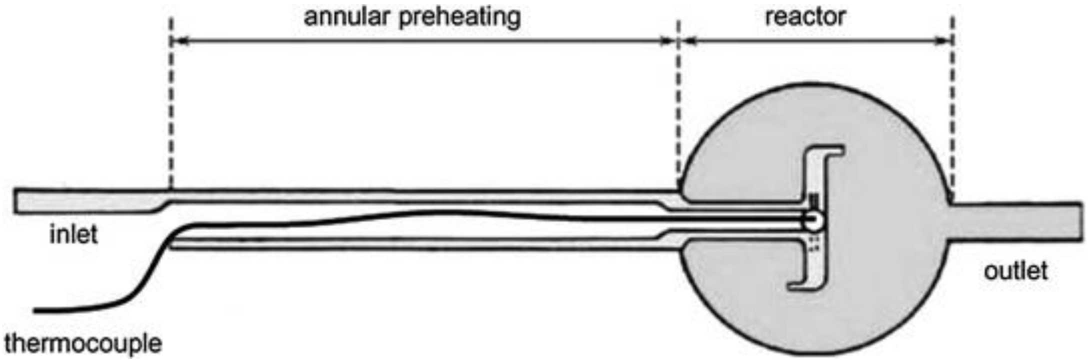

Figure 4: Jets located in the equatorial plane of the reaction volume.

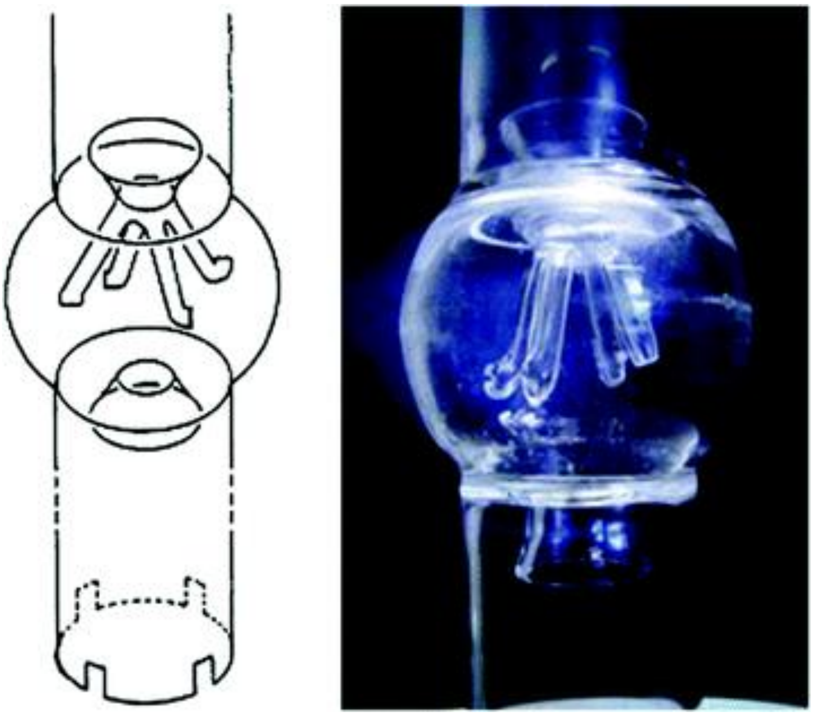

Figure 5: Jets have been angled downward to allow for investigation of the entire reaction volume. Holes drilled at bottom of exhaust to allow for pressure balancing.

the longitudinal axis of the reactor. According to literature review, jet stirred reactors have been used for gas-phased kinetic studies by a handful of researchers world-wide. De´partement de Chimie Physique des Re´actions in Nancy, France used a JSR for the study of the oxidation and pyrolysis of various hydrocarbons at atmospheric pressure[23] [24]. A high pressure JSR has been used by C. N. R. S. Laboratoire de Combustion et Syste`mes Re´actifs in Orleans, France for chemical kinetics studies of hydrocarbon oxidation[25] [26]. The Department of Physical Chemistry and Centre for Combustion and Energy at Leeds, England has used a form of a jet stirred reactor to study oscillatory ignition phenomena [27]. The Combustion Research Facility at Sandia National Laboratories in California and the National Synchrotron Radiation Laboratory at the University of Science and Technology of China, Hefei, Anhui couple a jet stirred reactor with synchrotron ionization techniques for low pressure oxidation studies[28, 29]. All of these reactors have worked to their specifications and produced impactful science, but also have some limitations on the physical conditions attainable, specifically pressure. Table 1 shows an overview of experimental conditions used for the jet stirred reactors mentioned above. Most of these experiments are conducted at a range of 1 – 10 atm with the exception of a few experiments conducted at 40 atm[1].

Table 1: Overview of experimental conditions used from recent JSR experiments[1].

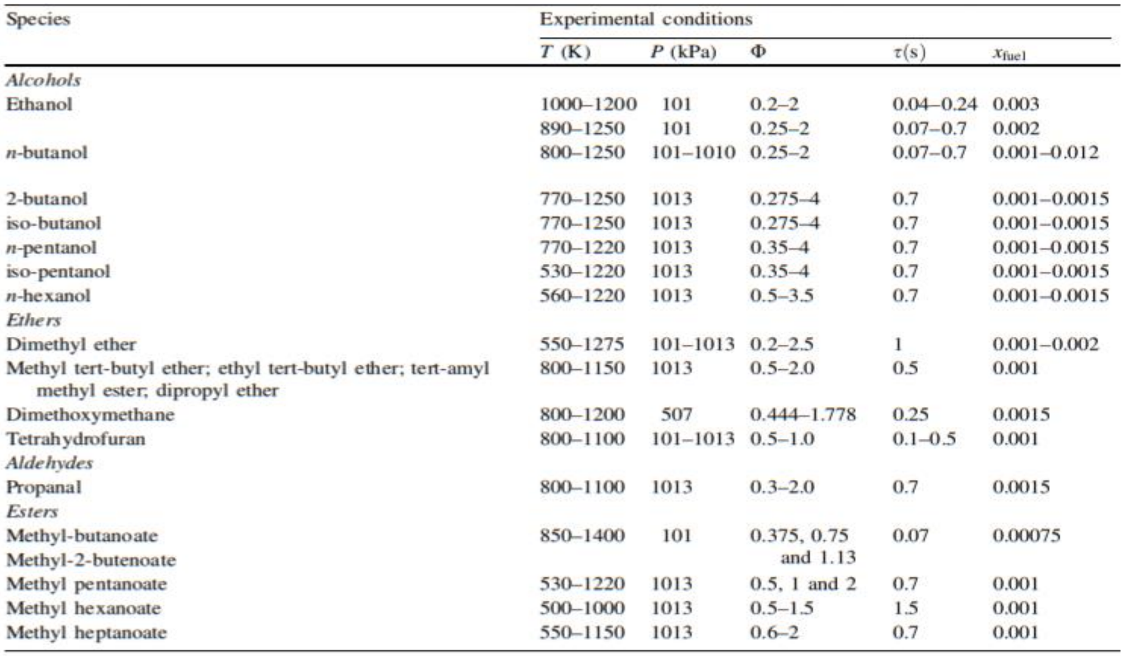

Species	Experimental conditions				
	T (K)	P (kPa)	Φ	τ(s)	x_{fuel}
Alcohols					
Ethanol	1000–1200	101	0.2–2	0.04–0.24	0.003
	890–1250	101	0.25–2	0.07–0.7	0.002
n-butanol	800–1250	101–1010	0.25–2	0.07–0.7	0.001–0.012
2-butanol	770–1250	1013	0.275–4	0.7	0.001–0.0015
iso-butanol	770–1250	1013	0.275–4	0.7	0.001–0.0015
n-pentanol	770–1220	1013	0.35–4	0.7	0.001–0.0015
iso-pentanol	530–1220	1013	0.35–4	0.7	0.001–0.0015
n-hexanol	560–1220	1013	0.5–3.5	0.7	0.001–0.0015
Ethers					
Dimethyl ether	550–1275	101–1013	0.2–2.5	1	0.001–0.002
Methyl tert-butyl ether; ethyl tert-butyl ether; tert-amyl methyl ester; dipropyl ether	800–1150	1013	0.5–2.0	0.5	0.001
Dimethoxymethane	800–1200	507	0.444–1.778	0.25	0.0015
Tetrahydrofuran	800–1100	101–1013	0.5–1.0	0.1–0.5	0.001
Aldehydes					
Propanal	800–1100	1013	0.3–2.0	0.7	0.0015
Esters					
Methyl-butanoate Methyl-2-butenoate	850–1400	101	0.375, 0.75 and 1.13	0.07	0.00075
Methyl pentanoate	530–1220	1013	0.5, 1 and 2	0.7	0.001
Methyl hexanoate	500–1000	1013	0.5–1.5	1.5	0.001
Methyl heptanoate	550–1150	1013	0.6–2	0.7	0.001

In summary, the lack of high-pressure experiments (above 40 atm) leaves a major gap in experimental data available. All of the design improvements mentioned above were included in the design of this reactor to create a JSR with the widest range of experimental parameters. The ability of this reactor to reach pressures greater than 50 atm this will allow for the unique ability to fill this gap and provide data that will strengthen the robustness of combustion models.

CHAPTER 3

FACILITY COMPONENTS

Along with a high-pressure jet-stirred reactor, several apparatus were designed and constructed in order to perform speciation analysis and create a complete chemical kinetics facility. The role of the various apparatus enable the transport, storage, and analysis of products formed, as well as provide supporting spectroscopy and mass spectrometry data *a priori* that is required for complete analysis of the reaction products, i.e. isomer resolution. The sections below are divided into two main categories: facility components that contain or analyze the reactive gas and facility components that provide absorption cross sectional data.

Figure 6 shows the flow of a fuel through the experiment. This is to provide clarity when the each of the individual components are references later in the paper. A

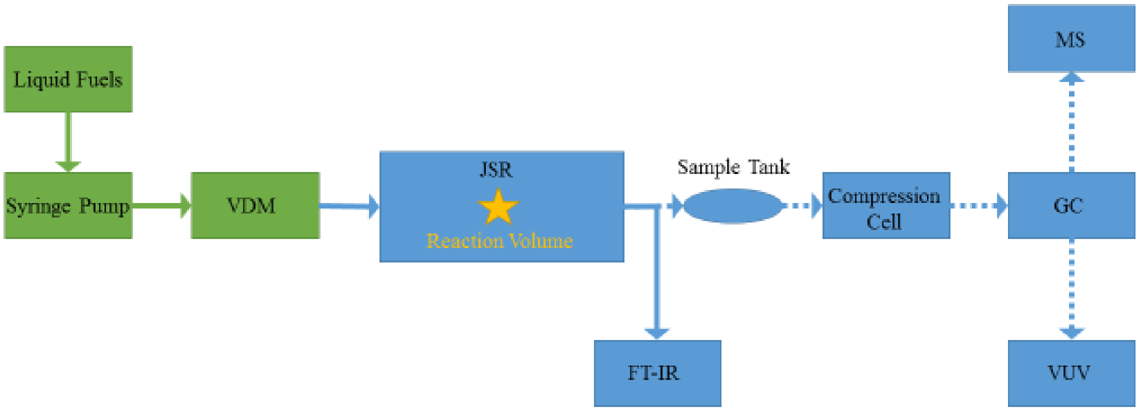

Figure 6: Flow of fuel through the reactor and facilitating equipment. Green denotes liquid phase, and blue gas phase. Solid line denotes continuous flow of gas while dotted line represents off-line analysis via portable sample tank.

volume of liquid fuel is fed into the vapor delivery module (VDM) via a syringe pump where the liquid is vaporized and mixed with nitrogen to form a saturated fuel vapor. This fuel vapor is then introduced into the jet-stirred reactor (JSR) where the fuel reacts at a specific temperature, pressure, and residence time. On-line FT-IR analysis is performed in real time. Samples are stored in portable sample tanks for transfer to the analytical equipment. Samples are then compresses and chromatographically separated into individual reaction products. These products are then analyzed simultaneously using mass spectrometry (MS), and electronic absorption spectroscopy (VUV).

Facility Components for Reactive Gases

After the gases have reacted in the reactor at a given residence time, on-line and off-line analysis is needed to determine the identity and concentration of the products formed during the reaction. An array of analytical techniques and apparatus were developed that enable the identification and quantification of the products formed. This data will allow for the development of reaction mechanisms, reaction rates, and other chemical kinetic data for hydrocarbons and biofuels.

The following sections discuss several components: FT-IR spectroscopy measurements, gas chromatography separation, thermal conductivity measurements, mass spectrometry measurements, electronic absorption spectroscopy measurements, and a compression cell used to deliver the gas to previous components.

FT-IR

The first method of analysis is the Shimadzu IRTracer-100 Fourier Transform Infrared Spectrophotometer (FT-IR). FT-IR is a technique used to obtain a spectrum of infrared absorption or transmission of a gas. IR radiation is not energetic enough to bring about electronic transitions encountered in UV or visible radiation, but instead causes changes in the vibrational frequency of the molecules bonds. Absorption only occurs when a molecule undergoes a net change in dipole moment as it vibrates or rotates. Certain molecular bonds will absorb specific wavelengths of infrared radiation. For example; a carbon–hydrogen bond will absorb infrared radiation around 2900 cm^{-1}, a carbon–carbon single bond will absorb radiation around 1100 cm^{-1}. The wavelength of the light introduced to the sample is controlled by a system of moving mirrors inside the FT-IR. These mirrors utilize constructive and destructive interference of the incidence light source to produce an interferogram. An interferogram shows signal intensity as a function of mirror position. The interferogram data is then converted to signal intensity as a function of wavelength using Fourier transform. FT-IR will allow for identification of simple molecules like CO and CO_2, and presence of function groups on more complex molecules. FT-IR will initially be use as a method of observing the formation of CO,

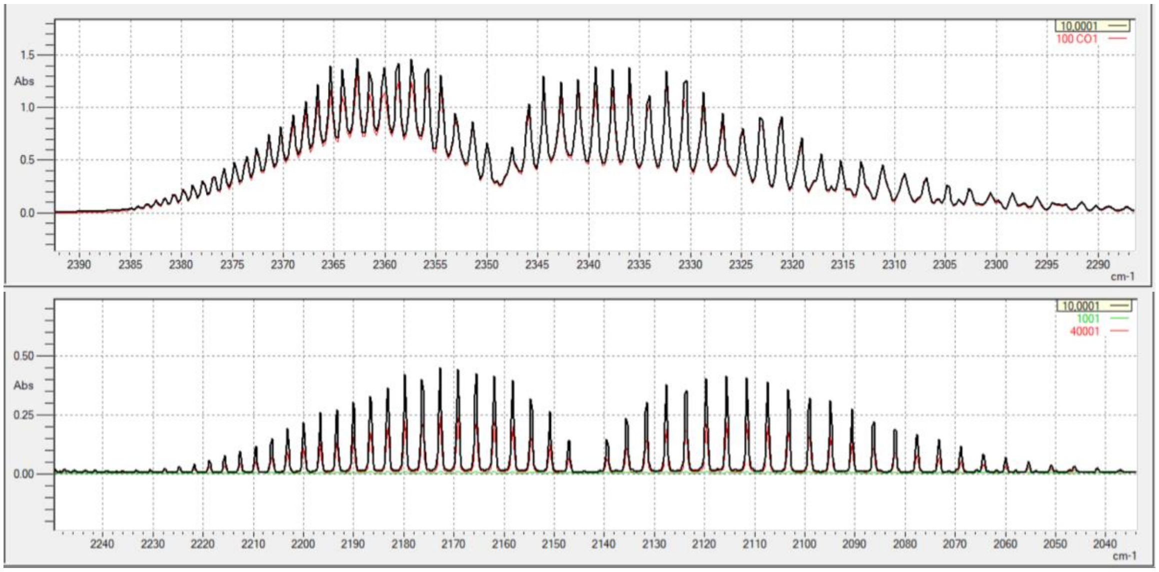

Figure 7: Top: absorption of CO_2 at 10,000 ppm; Bottom: absorption CO at 10,000 ppm

CO_2, and H_2O as a function of time inside of the reactor. CO, CO_2, and H_2O have very distinct absorption features that stand out when compared to hydrocarbons (Figure 7). The FT-IR will be located down-stream of the reactor. The reaction products will flow directly from the reactor to the FT-IR flow cell. Using a program called Time Course we will be able to analyze the absorption at a specific wavelength as a function of time (Figure 8). This will allow the relative concentration of CO, CO_2, and H_2O to be measured as a function of time. Once the signal from these molecules levels out and doesn't change over a set period of time the reactor can be described as operating in steady state. Figure 8 shows the absorption of methanol as a function a time. Once the absorption signal levels out around 500 s then the concentration of methanol inside the FT-IR flow cell has reached stead state. Experiments using pre-mixed gas samples and a bubbler were done on the FT-IR to determine time required to reach steady state are various concentrations, flow rates, and pressures. It was determined that regulating the back pressure of the FT-IR flow cell decreased the time for the absorption signal to reach a constant value. These experiments also revealed that heating of the FT-IR flow cell and

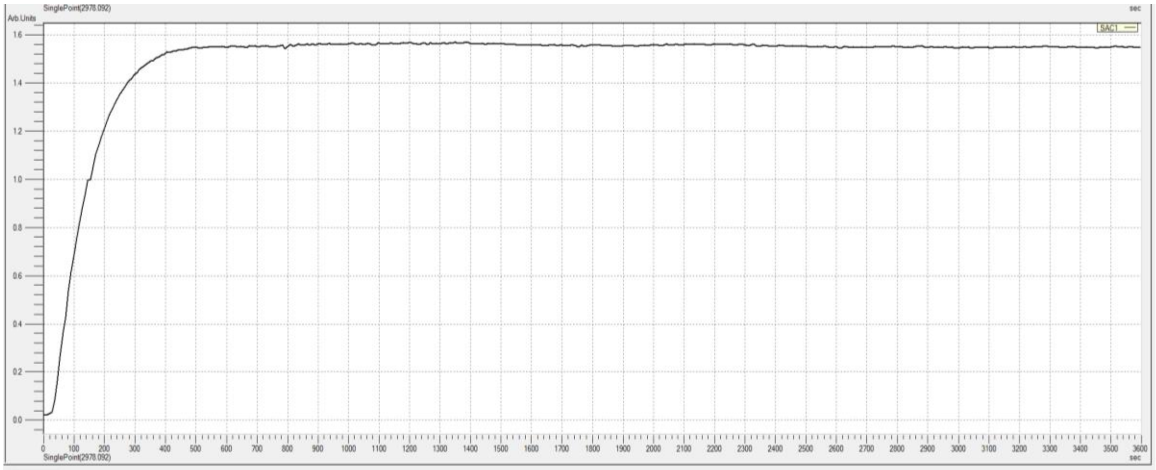

Figure 8: Absorption of methanol at 2986 cm^{-1} as a function of time

high flow rates (5 L/min) of purge gas (N_2) are required to sufficiently purge the FT-IR of previous experiments. Confidence of steady state is crucial if wanting to model this reactor under the continuous stirred-tank reactor assumptions. This is also vital information that will indicate when to extract a sample from the reactor for further analysis.

Gas Chromatography

Gas-phase samples extracted from the reactor will be of relatively unknown composition and will require chromatographic separation before any useful mechanistic information from combustion reactions can be inferred. In gas chromatography, the components of a vaporized sample are separated as a consequence of being partitioned between a mobile gaseous phase, gaseous sampling flowing through the column, and a stationary phase, viscous material held inside the column. Figure 9 shows a simple schematic of a gas chromatograph. Elution is brought about by the flow of an inert

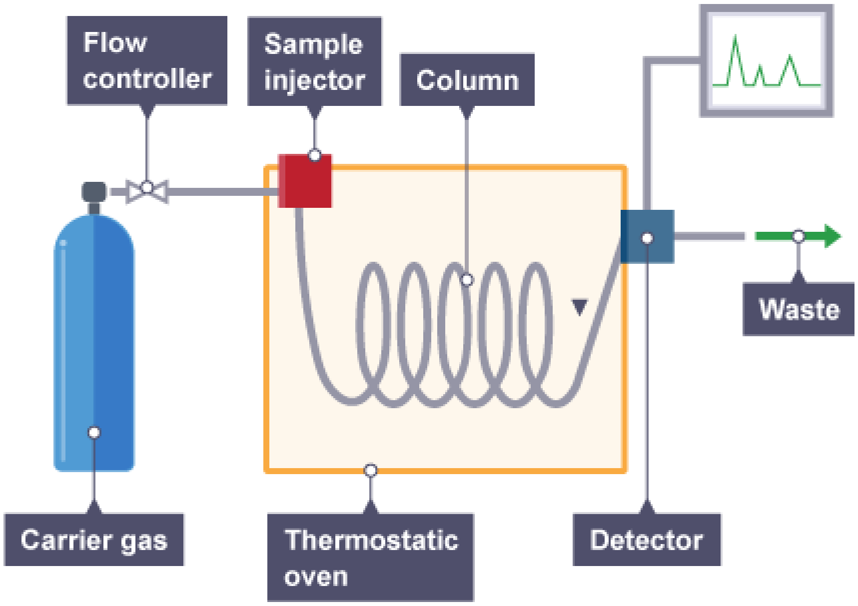

Figure 9: Schematic of a gas chromatograph.

gaseous phase. The mobile phase is an inert gas that does not interact with the analyte, and whose function is to transport the analyte through the column. For this project an Agilent Technologies 7890B GC system is used. This GC contains two identical columns that allow a single sample to be separated and injected into a mass spectrometer and an absorption spectrometer simultaneously. A single sample is split onto the two columns via a system of pneumatically actuated valves. This will allow for peak comparison at similar retention times. For example, at a retention time of 3 minutes a peak is detected by the mass spec showing a molecule with a certain mass is present. It is then known that the peak that shows up on the spectroscopy detector 3 minutes into the run is caused by a molecule with that particular mass. Potential products with that mass will then be theorized from known reaction schemes.

Thermal Conductivity Detector

While the sample flows through the valving system a third stream is produced and analyzed by a thermal conductivity detector (TCD), Figure 10. A TCD analyzes the difference in thermal conductivity between the sample and the carrier gas (He). The

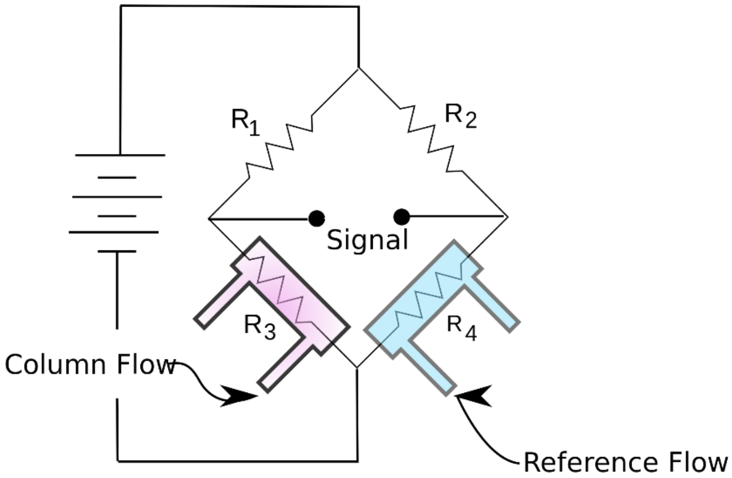

Figure 10: Schematic of a thermal conductivity

difference in thermal conductivity of the column flow versus as reference flow is quantified via a change in voltage across a Wheatstone bridge. This change in voltage can then be related to the concentration of various molecules. This TCD will be used to determine the presence of molecules like CO and CO_2. A steady signal from the TCD will also provide insurance that the composition of the sample is uniform. Any variation in TCD signal during a single run would indicate a leak or catalytic wall reactions inside the sample lines.

Mass Spectrometry

Mass spectrometry (MS) is a versatile and widely used tool for identifying compounds present in a sample. This technique is capable of providing information about the elemental composition of samples, qualitative and quantitative composition of complex mixtures, and isotopic ratios of atoms in samples. One of the two GC columns will feed the separated molecules into an electron-impact mass spectrometer, which ionizes gaseous samples at 70 eV. For this project an Agilent Technologies 5977B Mass Spectrometric Detector (MS) is used. This specific type of MS is a single quadrupole, which provides short scan times that are particularly useful for real-time scanning of chromatographic peaks. Most quadrupole mass spectrometers are divided into three main parts: the ionization source, the quadrupole, and the ion transducer. The ionization source is a stainless steel ribbon which emits electrons when heated that impact the gaseous sample with enough energy to ionize the molecule; stripping off an electron and giving the molecule a positive charge. A mass-to-charge ratio (*m/z*) is then created on each molecule. The quadrupole is made up of four parallel rods positioned opposite of each other that serve as electrodes. Voltages are applied to the quadrupole rods to create an electrical field that alters the flight path of the newly ionized molecules. Depending on the voltages applied to the quadrupole rods, a molecule will either flow freely through the center to reach the ion transducer and produce a signal, or strike the rods and become neutral molecules. This is a function of the molecules mass and is calibrated for known masses. Therefore, only ions having a limited range of *m/z* (mass-to-charge ratio) values will reach the detector. The charge for all of the molecules is +1 so the values recorded represent the mass of the molecule. The ion transducer collects the number of impacts that occurred and produces a signal for that specific *m/z* value. Figure 11 shows an example of an electron impact mass spectrum of an in-house reference gas that contains

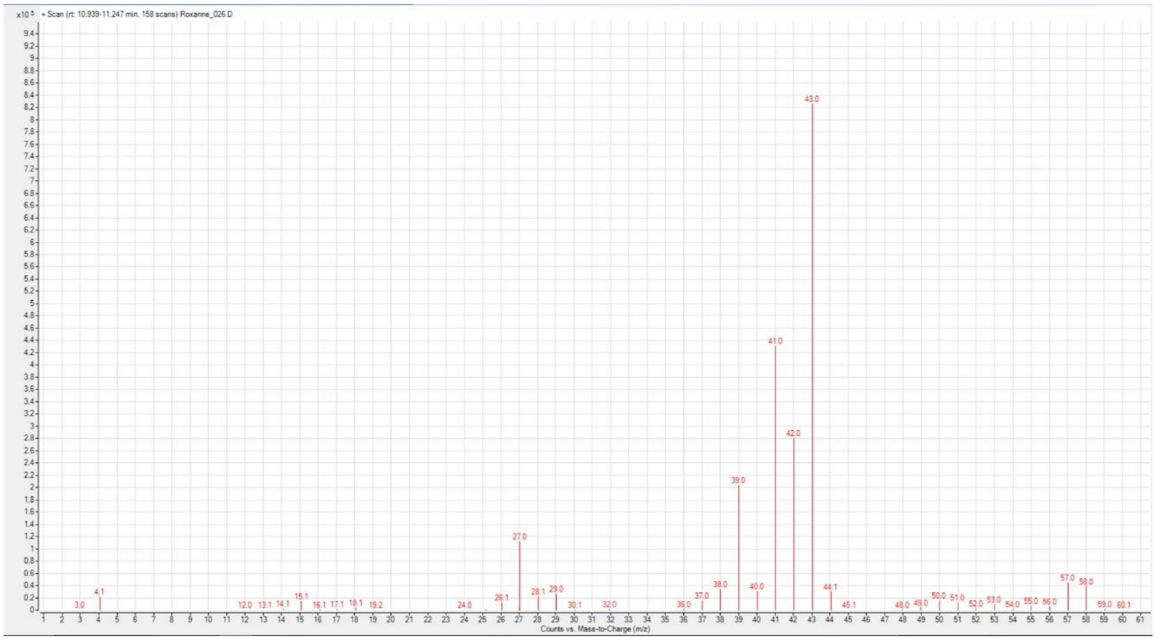

Figure 11: Mass spectra of an in-house reference gas containing CO, CO_2, and various hydrocarbons

certain target species. The magnitude of the peaks represents the relative abundance of molecules with that *m/z*. Due to the complex nature of low temperature combustion chemistry, many of the products produced from combustion experiments will be isomers of other products formed. This means that signal for multiple different molecules will show up as one peak in the mass spectrum. This is problematic when trying to develop a complete reaction mechanism for a certain fuel. To combat this problem electronic absorption spectroscopy is conducted in tandem with the MS to obtain isomeric resolution.

Electronic Absorption Spectroscopy

The fourth and final method used to determine the composition of our unknown samples is electronic absorption spectroscopy. This method is similar to FT-IR but key characteristics make this method much more sensitive to differences in molecular structure and chemical bonding. The spectroscopy diagnostic uses a deuterium (D_2) lamp as broadband light source. The spectral range is 115-240 nm (10.8-5.2 eV) with a resolution of 0.05nm. The main components of the spectrometer are the radiation source, flow cell, coated windows, grating, and detector. As opposed to the FT-IR, which uses moving mirrors to vary the wavelength of the light source prior to the sample flow cell,

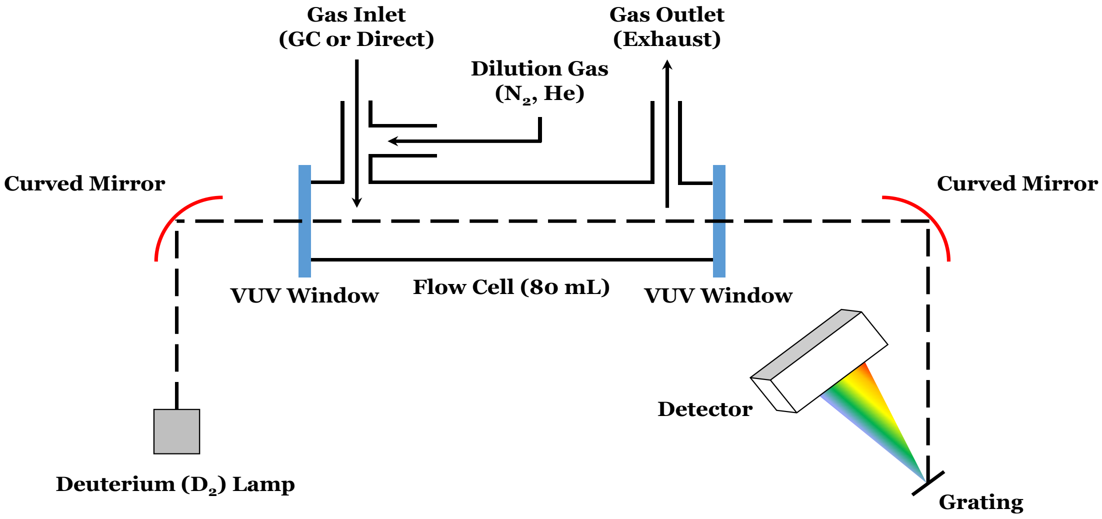

Figure 12: Overview of the electronic absorption spectroscope showing the light source, flow cell, grating, and detector.

the absorption spectrometer uses a grating after the flow cell to separate the light (Figure 12). The diagnostic provides absorption cross-sections over a range of energy for the molecules in question. The absorption cross-section of a molecule describes the magnitude of absorbed light at a specific wavelength. The absorption cross-section measurements are conducted in a temperature and pressure controlled environment using Beer-Lambert law (Equation 3). $I(\lambda)$ and I_0 are the final and incident light intensity determined. $\sigma_i(\lambda)$ is the absolute absorption cross-section of the sample molecule. c_i and L are the concentration of the molecule in the sample and path length of the light respectively. The path length is determined by the flow cell, which is fixed at 10 cm.

$$I(\lambda)/I_0 = exp(-\sigma_i(\lambda)c_iL) \tag{3}$$

Absolute absorption cross-sections are the extracted from the Beer-Lambert law (Equation 4).

$$\sigma_i(\lambda) = (c_iL)^{-1}\ln I_0/I(\lambda) \tag{4}$$

While the unknown samples will be chromatographically separated, there is still a chance that multiple species will exit the GC at the same time. For absorption signal comprised of multiple species, fractional contributions $A_i(\lambda)$ from individual species to the total spectrum $A(\lambda)$ are determined using non-linear regression analysis to produce an optimized and distinct set of fitting coefficients, f_i (Equation 5).

$$A(\lambda) = \sum_{i=1}^{N} A_i(\lambda) = \sum_{i=1}^{N} f_i\sigma_i(\lambda) \tag{5}$$

The Beer-Lambert law also allows for the concentration of the products to be determined. This requires the cross sections, at a known concentration, to be measured for any species that requires quantitative data. A library of cross-sections measurements of different molecules relevant to combustion and atmospheric chemistry is under development. Once this library is completed, comparison between cross-sections of reaction products and known cross-sections at known concentrations will determine the identity and concentration of the sample.

Absorption cross-sectional measurements are molecule specific, meaning even the smallest differences between two molecules will yield remarkably different cross-sections. This feature allows these experiments to be extremely sensitive and have isomeric resolution. Figure 13 shows the differences between the cross-sections of *cis*-butene and *trans*-butene.

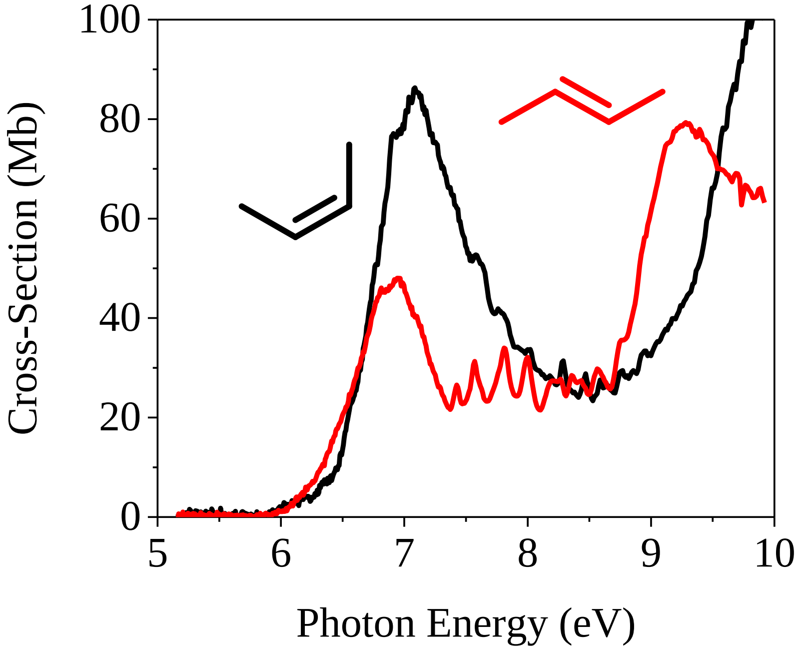

Figure 13: Absorption cross sections for *cis*- butene and *trans*-butene

Isomeric resolution is extremely important in low-temperature combustion experiments. At these low temperatures (400 - 1200 K) the molecules tend to isomerize more readily, as compared to higher temperatures where the molecules almost instantly break down to CO_2 and H_2O. Determining whether or not a certain combustion reaction favors the formation of one isomer over the other can have a major impact on the reactivity and energy release of the reaction.

Compression Cell

Once the sample has been collected and stored in the sample tank (Figure 6), the tank will be disconnected and prepped for analysis. The tanks will contain roughly 100 – 200 Torr of sample. In order to extract the sample and supply it through the GC for chromatographic separation it first must be compressed above atmospheric pressure. To do this, an aptly named compression cell was designed and built (Figure 14). This cell consists of a static housing and a dynamic piston controlled by an electronically controlled actuator (IAI RCP5-RA10R ROBO Cylinder). All the parts of the cell and piston are made of 304 stainless steel and coated with an inert coating called Dursan. The

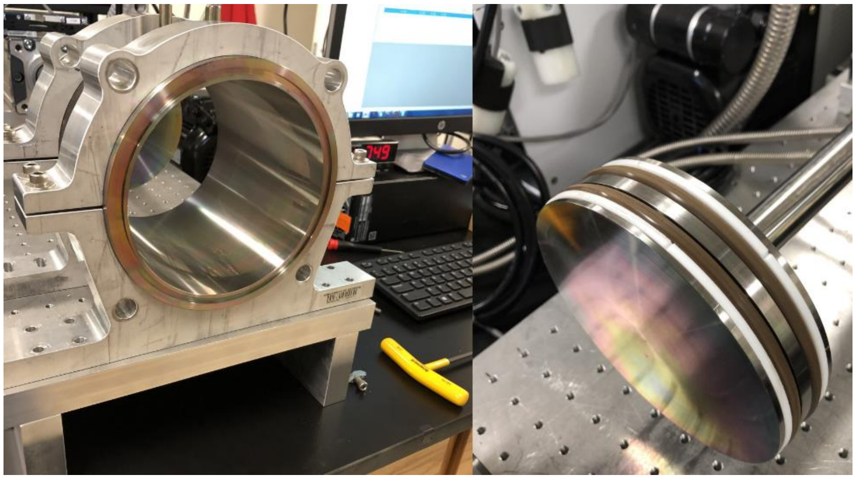

Figure 14: Left: Compression cell body; Right: Compression cell piston with double X-ring seal connected to actuator rod

internal volume of the cell ranges from 6563.8 cm^3 when fully retracted to 506.7 cm^3 when fully compressed. The maximum stroke length is 128 mm. Vacuum and sample inlet ports are located on top of the housing and controlled by coated quarter turn valves (Figure 15). Temperature/pressure measurement and sample outlet ports are located on the front face of the housing and controlled by similar valves.

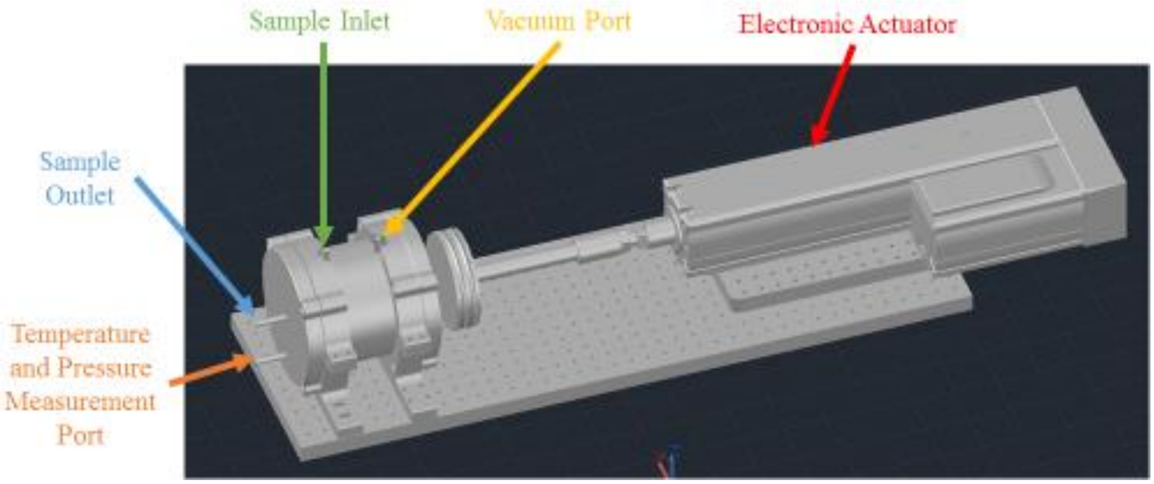

Figure 15: Schematic of compression cell and electronic actuator

Limiting the possible sources of contamination is important for any experiment. Because of this, the compression cell was designed to operate without lubrication. Many lubrications are hydrocarbon based and could contaminate the hydrocarbons in the sample. In order to create a perfect seal between the dynamic piston and static housing without lubrication, the edge of the piston contains two X-rings that each provide two points of contact (Figure 16). X-rings were chosen to reduce the friction created when the piston is moving. A leak rate test determined that the X-rings were able to hold a vacuum for over 48 hours. The leak rate test was conducted by pumping the compression cell down to vacuum with a roughing pump. The compression cell was then sealed via the

Figure 16: Cross section of an X-ring. Showing two points of contact

valves on all the ports and left over 48 hours. After 48 hours there was no rise in pressure; confirming the compression cell was properly sealed.

It was determined that compressing the sample to a pressure of 1520 torr, or 2 atm, was sufficient for delivery to the GC to provide several purges of sample gas prior to initiating the GC method that begins the analytical procedure. Figure 17 shows the stroke length required to reach 1520 torr for various internal pressures. To extract the sample from the tanks the piston is fully retracted and vacuum is drawn on the compression cell. The sample tank is then opened and the sample is allowed to flow freely into the compression cell. Based on Figure 17, the pressure inside the cell must be at least 50 torr at this point in order to reach 1520 torr with the available stroke length. Compressed pressures between 760 and 1520 are adequate for flow to the GC, but limit the amount of sample that is analyzed. The system utilizes the signal output from the pressure gage and a programmable logic controller (PLC) to control the movement of the actuator. Once initiated, the actuator will push the piston until the internal pressure reached 1520 torr, or

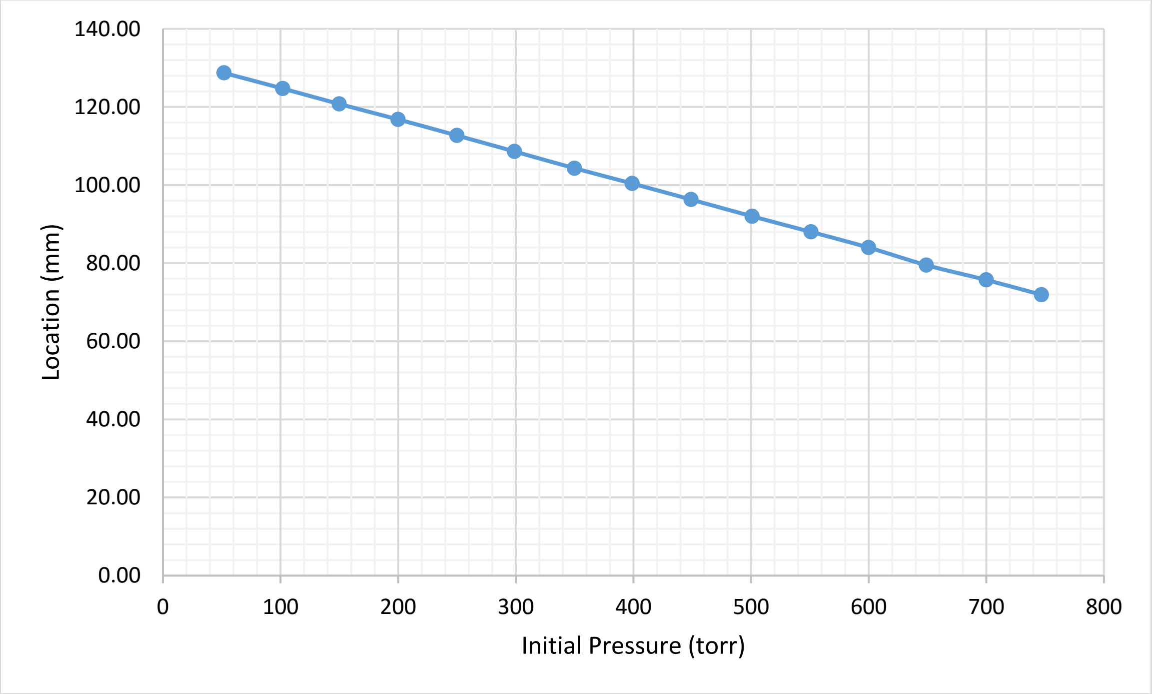

Figure 17: Stroke length required to reach 2 atm starting at various initial pressures.

until the piston has reached its maximum stoke length. Small portions of the sample are then extracted and sent to the GC for separation. If the internal pressure ever falls below 1520 torr the actuator starts to push the piston until the target pressure is reached again; providing a constant pressure at the inlet of the GC.

Below is a summary of the steps required to compress a gas sample:

1. Make sure the piston has been retracted to its "home" position opening the compression cell.
2. Close all valves except the temperature and pressure measurement port and sample outlet port. Make sure valve near GC inlet is closed.
3. Use roughing pump to pump the compression cell to near vacuum.
4. While the compression cell is pumping down, connect the sample take to the inlet section (convoluted tube).

5. After cell has been pumped down close the sample outlet port and open the sample tank and allow the sample to flow into the compression cell. The pressure should read at least 50 Torr at this point to make sure 1520 Torr is reached with available stroke length.
6. Close valve to inlet and vacuum ports.
7. Flip switch on PLC to initiate compression.
8. Compression will stop once 1520 Torr inside the cell is reached.
9. Open the sample outlet port and allow sample to flow to GC inlet.
10. Once ready to introduce the sample to the GC open the valve to the GC and start the method
11. Compression will start automatically if the internal pressure of the cell drops below 1520 Torr during sampling.
12. Once sampling is complete flip the switch on the PLC to stop the compression program.
13. Retract the piston back to its “home” position.
14. Close sample outlet port
15. Open sample inlet and vacuum ports and allow vacuum to purge compression cell and sample tank.

Facility Components for Cross Section Measurements

Along with the analytical techniques mentioned above, an array of apparatus were designed and built to facilitate species identification and quantification of reaction experiments by providing fundamental spectroscopic and mass spectrometric data. These tools serve to provide initial data required for these experiments. High-accuracy gages were chosen and carful methodologies were developed to ensure precision of these apparatus.

Gas Manifold

The Beer-Lambert law used to determine the cross section requires the concentration of a sample molecule to be known. Cross-sections are essential for determining the identity of an unknown molecule and are a function of the concentration of the molecule as well as wavelength for a given path length. Developing a concentration curve for target species allows the concentration of those species in a sample to be determined. This requires cross-section measurements to be taken for all hypothesized products over a range of concentrations. To do this, mixtures need to be made and analyzed for every compound over a range of concentrations. While this is a daunting task, combustion products can be predicted using the widely accepted low temperature combustion reaction scheme to help narrow the search window (Figure 2). A gas manifold, Figure 18, is used to create mixtures with a known concentration. This manifold uses a vacuum pump, 5000 Torr pressure transducer, 10 Torr pressure transducer, and a supply tank of He to create mixtures. The freeze, pump, thaw method is used to remove unwanted gases prior to mixture making and in some cases provide further sample purification. The approach to making mixtures is as follows. First, attach an empty sample tank to the manifold and allow to pump down to vacuum overnight. This ensures the tank is completely empty and reduces chance of contamination. Next, after closing the valve to the tank place a small amount of liquid sample into glass vial and attach to the gas manifold using an ultra-Torr fitting. Making sure to keep the valve to the vial closed to prevent air from entering the manifold. Fill-up the dewar (Figure 19)

Figure 18: Manifold used to create gas phase mixtures of hypothesized products at known concentrations

with liquid nitrogen (LN2) and freeze the liquid sample inside the glass vial. Next, open the valve to the vacuum pump and the valve to the vial to allow the pump to draw all of the excess atmospheric air out of the manifold. Freezing the sample with LN2 lets the atmospheric air to be pumped out without pumping out the sample itself. All excess air is gone when the 10 Torr gage reaches a minimum near zero (e.g. 0.0015 Torr). Close the valves to the vacuum pump and the sample vial. Remove the LN2 and allow the sample to thaw. Open the valves to the tank and sample vial allowing the sample vapor to fill the manifold and tank. The pressure gages will read the pressure of the vapor inside the manifold and tank; be mindful to close the valve if exceeding the limit of the 10 Torr gage. Once the desired pressure, or vapor pressure, is reached close the valves to both the tank and the glass vial and record the pressure inside of the tank. Open the system to vacuum and allow all of the excess vapor inside the manifold to be pumped out. Once the pressure reaches the zero value close the valve to the 10 Torr gage. Slowly open the helium inlet to allow helium to flow through the manifold until the 5000 Torr pressure gage levels out around 80 Torr. Helium is used here because it does not absorb radiation in the 125 – 240 nm wavelength range. Next, quickly close the valve to the vacuum and then open up the valve to the tank. Make sure the pressure inside the manifold is greater than the vapor pressure value recorded earlier before opening the valve to the tank. Allow the pressure to rise until the desired pressure. Close the helium inlet and then quickly close the tank valve. Record this final pressure before slowly opening the vacuum. Leave the tank to sit overnight to allow adequate mixing time.

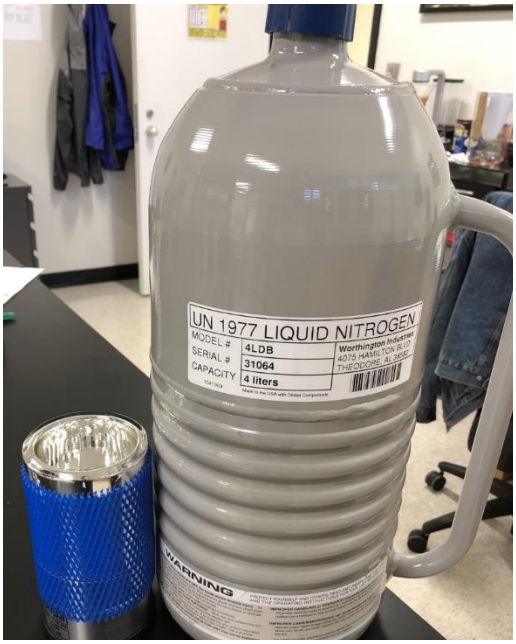

Figure 19: 4L LN2 dewar (right) used to store LN2 in lab. Smaller LN2 dewar (left) used with the gas manifold

Two pressures are recorded during this procedure. Dalton’s Law (Equation 6) is used to relate the contributions from each species to the total pressure of the tank. In a volume-based application the concentration c_i can be determined by the partial pressure of the species and the total pressure (Equation 7). For example, when filling a tank initially with 50 Torr of cyclohexane and pressurized with helium to 5000 torr. The tank would contain a 1% mixture of cyclohexane.

$$P_{Total} = \Sigma P_i \qquad 6$$

$$P_i = P_{Total} c_i \qquad 7$$

The entire manifold is wrapped with seven resistance heating wires to prevent condensation of sample on the inside walls of the manifold. Each pair of wires are controlled by an Omega R90033 PID controller and two K-type thermocouples. These controllers continuously maintain the temperature around a set point of 60 °C. If the thermocouple reads a temperature higher or lower than the set point it will either provide or cut off power to the heating cords. The sample tanks are also kept in custom heating jackets controlled with a PID and thermocouple that maintain the tank at a similar temperature. Keeping a constant temperature is important to prevent differences in pressure readings at various points in the manifold and tank. Once the mixture is made, the tank can be disconnected and attached to the cross-section manifold for injection into either the absorption spectrometer or the gas chromatograph for mass spectrometry analysis.

Cross-Section Manifold

The purpose of the manifold is to deliver a precise amount of pre-mixed gases into both the GC and absorption spectrometer at constant temperature and pressure. The cross-section manifold consists of a mass flow controller (MFC) positioned upstream of the inlets to both the GC and absorption spectrometer, a downstream pressure transducer and pressure controller positioned at the exhaust of the latter, and heating cords to prevent condensation. The heating cords serve a similar purpose to the gas manifold and are kept at a similar temperature to achieve the main goal of avoiding sample condensation. Since uniform temperature within a few degrees is less important on the manifold as compared to the reactor, the heating cords are all controlled by a single Variac transformer.

The temperature of the manifold is monitored by six thermocouples placed in key positions (Table 2). The MFC controls the amount of sample introduced to the absorption spectrometer. The pressure controller and pressure transducer work together to maintain pressure inside the VUV flow cell. The pressure controller will open or close a needed valve to maintain the pressure near the set point. Downstream of the pressure transducer the manifold is connected to a vacuum pump. This pump draws away the exhaust and can be used to pump down the manifold between samples.

Table 2: Position of thermocouples on cross-section manifold

Thermocouple	Position
1	Sample Inlet
2	Directly Downstream of MFC
3	Sample Outlet to VUV
4	Sample Outlet to GC
5	Pressure Regulating Valve
6	Outlet of VUV

Vapor Delivery Module and Syringe Pump

One of the main requirements for a potential biofuel is transportability. This usually means the fuel must be a liquid at room temperature and atmospheric pressure. In practical combustion systems, liquids are then vaporized inside of the engine prior to combustion. With the exception of methane, ethane, propane and butane that comprise natural gas, most of the purified compounds that will be tested in this reactor start off in the liquid phase. A Bronkhorst Vapor Delivery Module (VDM) is used to deliver a controlled amount of vaporized fuel into the reactor. The VDM consists of a Coriolis-type liquid flow controller, a mass flow controller for carrier gas, and a temperature controlled mixing and evaporation device. The liquid flow and carrier gas meet inside the heated mixing and evaporation device. Here, the liquid is vaporized and saturates the carrier gas. The saturated carrier gas then flows out of the device and into the inlet of the reactor. This device can generate saturated vapor within the range of 50 sccm to 10 L/min. The VDM is supplied by a Chemyx Fusion 6000 Programmable Syringe Pump that delivers a constant supply of liquid fuel to the VDM.

CHAPTER 4

DESIGN OF THE JET-STIRRED REACTOR

The primary goal of re-engineering the JSR was to broaden the range of experimental parameters, like temperature and pressure, to more accurately simulate in-engine conditions. A secondary goal was to provide ease of use to the experimentalist. Previous JSR have been oriented in the vertical direction. The quartz reactor, heaters, and probes were assembled outside the pressure chamber and then lowered into place. To perform any maintenance on a reactor like this everything must be removed and taken apart. This can be cumbersome and time consuming for the user. This was one of the main points that was taken into consideration when designing this reactor and the motivation for a horizontal design. The top lid can be removed to reveal the insulation, heating system, and reaction volume. The heating system and insulation have also been design in two halves to allow the parts to be removed from the top of the reactor. This allows the user to see and perform maintenance on the internal portions of the reactor without taking apart the whole system. Apart from ease of use, the reactor, Figure 20, was designed to reach experimental conditions that, until now, were unreachable in comparable reactors. This was done by re-designing the conventional approach to the heating system and utilizing pressure balancing for high pressures. With these modifications this reactor will be able to provide much needed experimental data for low-

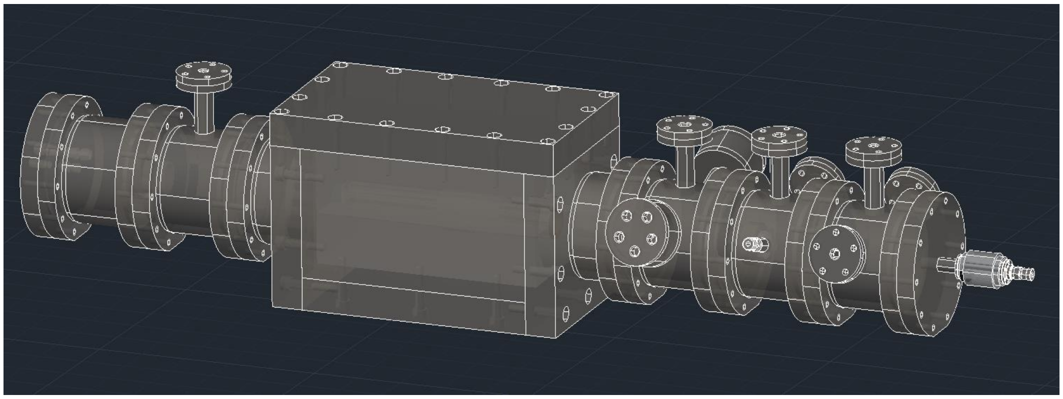

Figure 20: CAD model of the pressure chamber housing the JSR.

temperature and high-pressure combustion. In this section, each part of the reactor is described in detail.

Quartz Reactor

The quartz reactor is the long tube-like structure where the combustion reactions will take place. The quartz reactor contains the reaction volume, and both up-stream and down-stream sections. Quartz was chosen for its high melting point and chemical inertness. The melting point of quartz is around 1923 K which insures the structural integrity of the reactor will not be compromised at the higher temperature. The inert qualities of the quartz will insure any unwanted wall reactions are kept to a minimum. The defining characteristic and namesake of the JSR is the mixing jets located inside the reaction volume Figure 21. These four jets induce turbulent mixing inside the reaction volume ensuring homogeneity of the composition, which relies on the three main criteria[1]

- The jets from the four nozzles must be turbulent.
- The four jets must be able to provide intense internal recycling streams.

- The velocity of the jets at the outlet of the nozzles must not exceed the speed of sound.

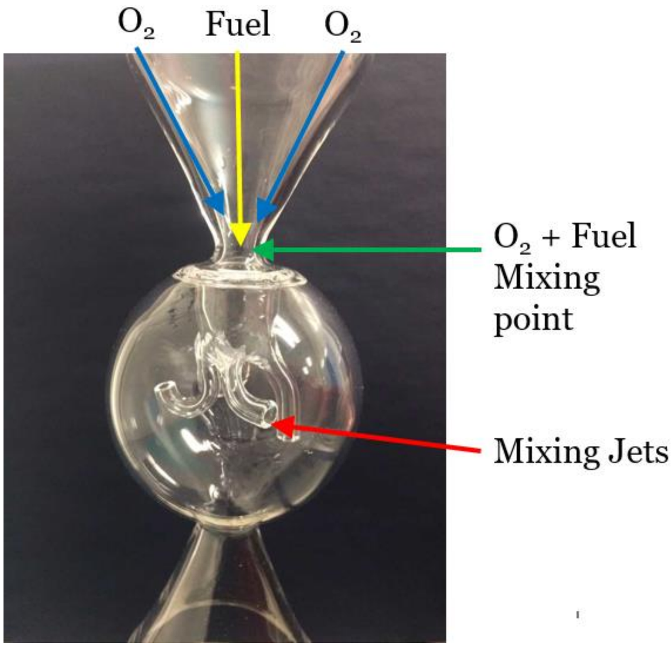

Figure 21: Reaction volume and mixing jets

The first criteria focuses on the Reynolds numbers of the gas exiting the jets. A Reynolds number greater than 800 is required to good mixing according to Herbinet and Dayma in Cleaner Combustion[1]. This sets an upper limit for the residence time of the reactor. The third criteria states that the velocity of the gas exiting the nozzles much be lower than the speed of sound for the temperature and pressure of the reaction. The velocity can be expressed as a function of radius of the reactor, diameter of the nozzles, and the residence time. Since the former are fixed geometries of the reactor this provides the lower limit of the residence time. Further analysis of homogeneity is discussed in Cleaner Combustion pages 183 - 210[1].

The dimensions of the quartz reactor are shown in Figure 22. The quartz reactor rests horizontally inside the stainless steel chamber and gas flows from left to right in relation to Figure 15. The spherical reaction volume, located in the center of the reactor, has a volume of 30 cm^3. This volume was chosen to accommodate a balance between residence time and internal surface area. A large internal surface area relative to the internal volume will increase the effect of wall reactions. Shorter residence times can be achieved with a smaller reaction volume, but the internal surface area-to-volume ratio will increase. A larger reaction volume will limit the effect of wall reactions, but significantly hinder the control of residence time. The upstream (left) side of the reaction was made slightly longer than the downstream (right) side to accommodate the pre-heaters. The upstream section converges towards the reaction volume to guide the O_2/N_2 towards the reaction volume.

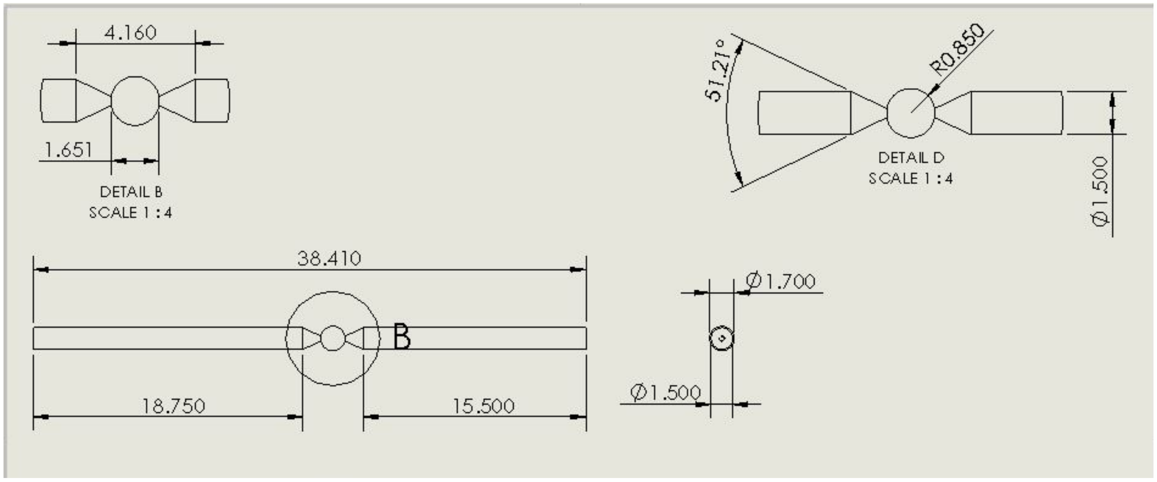

Figure 22: Dimensions in inches of the quartz reactor.

Modular Design of the Reactor Housing

To enhance the robustness of the reactor, a modular design methodology was adopted. Modular design is an approach that subdivides a system into smaller parts that can be used in different systems. This reactor was designed in six distinct sections that each work together to achieve the experimental goals, but can be easily switched out for a different section if those goals change in the future. Each section is made of 1" – 1.75" stainless steel and seal to the adjacent section with standard 5" O-rings. All feedthroughs into the reactor are ¼" National Pipe Thread (NPT) fittings. Since NPT is a national standard, this is a convenient and cost effective method to attach hardware to the reactor. The different sections can replace one another to further increase the experimental capabilities of the reactor. This design process was implemented with to allow the core pressurized chamber to be adapted to future experimental plans in atmospheric chemistry and multi-phase combustion. Science is an ever changing field and combustion chemistry is no exception. Hopefully this reactor will be in use for the foreseeable future, and this modular design will help modify its capabilities to fit the current need of the combustion community.

Reactor Housing: Sections 1 & 2

Section 1 serves at the inlet of the reactive gases and directs them through the quartz reactor. The fuel mixed with a carrier gas will be injected through the center port on the front faceplate directly into the capillary tube, which delivers fuel down the length of the reactor to the O_2 + fuel mixing point directly before the mixing jets. The O_2 and the N_2 carrier gas will be injected through off-center port located on the front faceplate (not-pictured). This gas mixture will fill the volume of Section 1 and flow down the length of the quartz reactor on the outside of the capillary tube. A 1.5–in. ultra-Torr fitting seals around the end of the quartz reactor separating sections 1 & 2. Section 2 serves as the inlet of the balance gas, and housing for the pre-heater and insulation. The gas balances the pressure on either side of the quartz reactor to insure the quartz does not break during high-pressure experiments.

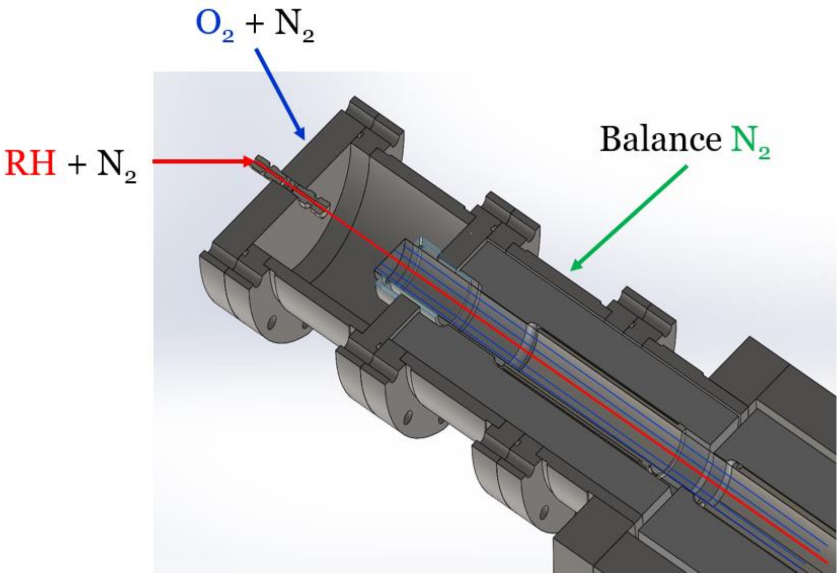

Figure 23: Sections 1 & 2 of the reactor housing.

Reactor Housing: Section 3

Section 3 holds the reaction volume, both heating elements, and the ceramic insulation. The stainless steel housing in Section 3 is 1.75” thick to accommodate the high pressure experiments. The extra thickness, compared to the cylindrical sections, is needed because square shaped volumes do not distribute the internal pressure forces as well as cylinders. A lid is located over the rectangular portion and sealed via O-rings. This lid can be removed to reveal the ceramic insulation, heating elements, and reaction

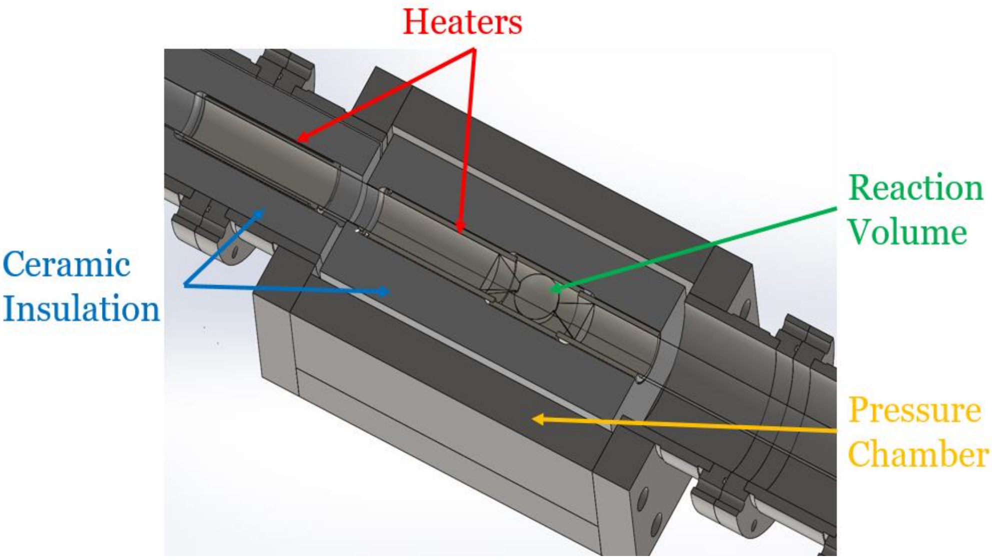

Figure 24: Section 3 of the reactor housing.

volume. The ability to see and reach inside the reactor allows the user to position the capillary tube, sonic probe, power supply wires, thermocouple wires, and heating elements quickly and easily. This approach is novel to this design and will greatly increase the ease of use of the reactor.

Reactor Housing: Sections 4, 5, & 6

Section 4 houses the electrical feedthroughs and the exit of the balance gas. The power supply cables for the heating elements and the thermocouple leads will travel from Section 3 to one of ten designated ports located on Section 4. These ports will have various sized compression fittings that will seal around the wires; 3 mm fittings for main heater supply cable, 2 mm fittings for the pre-heater supply cable, and 1.5 mm fittings for the thermocouple leads. The 1.5 mm fittings allow three thermocouple leads to be fed through a single, common port. Each of the four heating wires has two leads and each of the six thermocouples has a single lead for a total of required feedthroughs. Contrasting

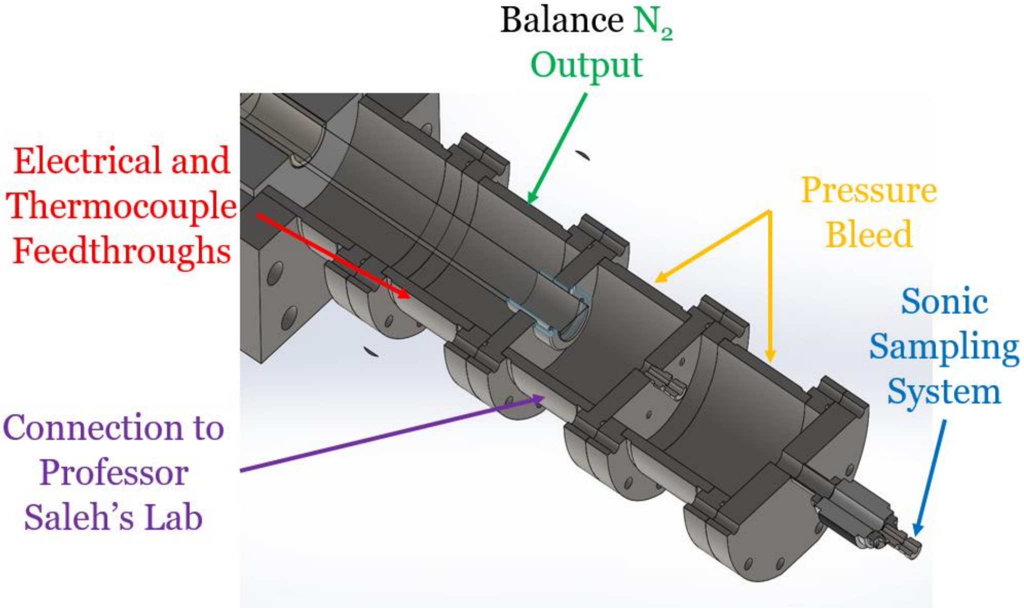

Figure 25: Sections 4, 5, & 6 of the reactor housing.

Section 2, the balance gas will exit via a port located in Section 4. Similar to the seal between Sections 1 and 2, a 1.5–in. ultra-Torr fitting is used to seal the end of the quartz reactor separating Sections 4 and 5. Section 5 contains a port that will be used to sample exhaust gas for aerosol particle analysis in collaboration with Professor Rawad Saleh's group at UGA. Section 5 and 6 will experience the bulk of the gases flowing through the quartz reactor with the exception of the sample extracted from the reaction volume. The linear motion thimble, motion controller for the sonic sampling system, is not rated for high pressures. Sections 5 & 6 will gradually decrease the pressure, via ports open to the atmosphere, making sure that the linear motion thimble does not experience any high pressures. All openings, ports, and feedthroughs can be plugged when not in use.

Heating System

Combustion reactions are broadly classified into three main temperature regimes: low temperature (500 – 900 K), intermediate temperature (900 – 1200 K), and high temperature (1200 – 3000K). High-temperature combustion is typically defined as the region where thermal decomposition, soot formation, and production of nitrogen oxides dominate[30]. Intermediate and low temperature combustion, however, display rich and complex isomer-specific chemistry that dictates many of the observed phenomena. These regimes are pressure and species dependent so building a reactor with a wide range of experimental conditions is essential. Figure 26 shows a ChemKin simulation of the formation of ethanol during the oxidation of diethyl ether[31]. The model was taken from Serinyel et al. that studied the oxidation of diethyl ether in a jet-stirred reactor at temperatures ranging from 450 – 1250 K, and pressures ranging from 1 – 10 atm. This figure demonstrates that even small changes in the experimental temperature can have drastic effects on the products produced and the rate of the reaction. Confidence in the exact temperature of the experiments is key to producing reliable data for these types of experiments.

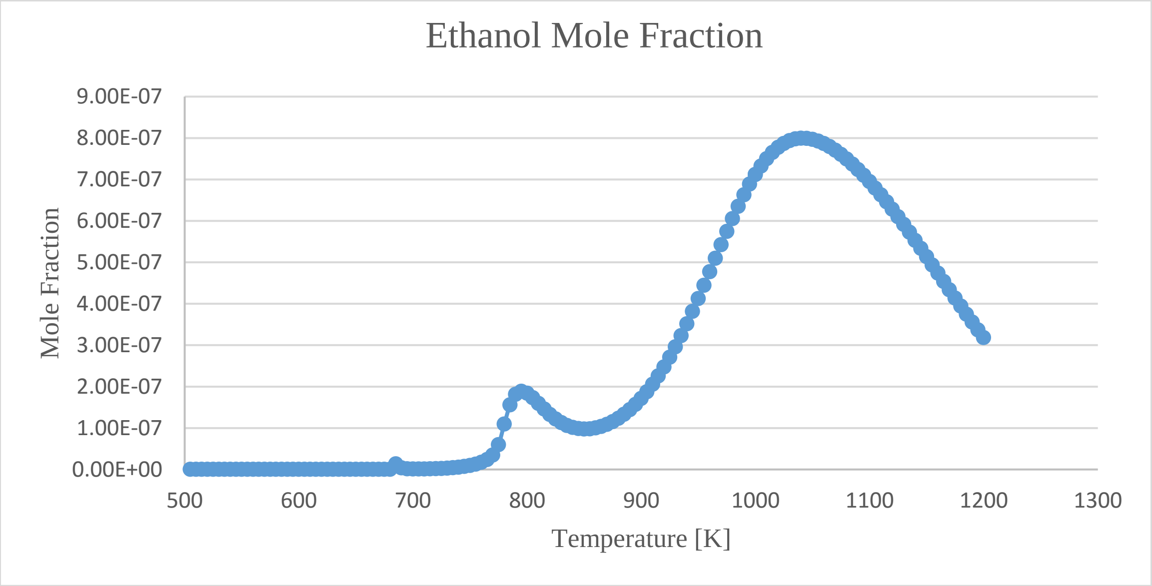

Figure 26: Ethanol formation from the oxidation of diethyl ether oxidation. Simulation done using a PSR at 1000K and 10 atm.

Early jet-stirred reactors used resistant heating wires to achieve the temperatures necessary for their experiments. The wire was wrapped around the reaction volume and an upstream pre-heating area and controlled with a variable voltage source. Including a pre-heating region proved to reduce the large temperature gradients in the reaction volume that were present in experiments without a pre-heating region[16]. Variations in wrapping patterns and cold spots created by the gaps in the heating wire led to questions regarding the thermal homogeneity inside the reaction volume. The heating system of this reactor was re-engineered to insure homogenous temperature inside the reaction volume and therefore the validity of the experiments. A temperature gradient of < 1.0 K across the radius of the reaction volume is considered homogenous. Figure 27 shows the location of the heating elements in the reactor.

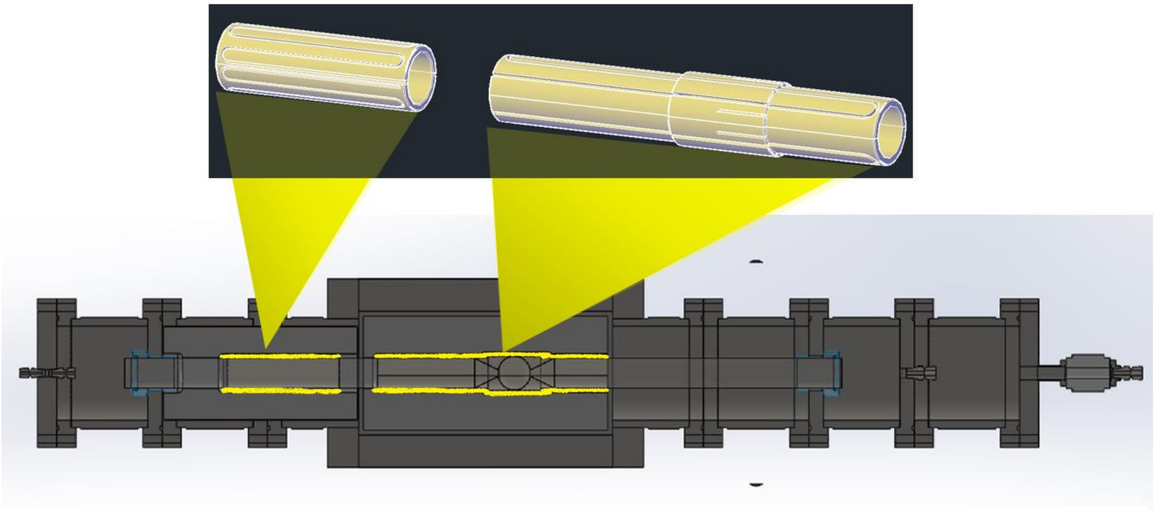

Figure 27: The position of the pre-heating and main heating elements in relation to the reactor housing

The initial design of the heating system aimed to fix the issue of the cold spots created by the gaps between the heating wires and variations in wrapping techniques, while still maintaining ease of access to the internal workings of the reactor. Permanently affixing the heating wire into grooves in a ridged body surrounding the reaction volume solves the problem of wrapping variations. The initial design considered using two copper half-cylinders, serving as the ridged body, would allow the heat to spread out and provide a uniform heat source around the spherical reaction volume. Copper was initially chosen for its unparalleled thermal conductivity (*k* = 401 W/m K), with the idea of minimal heat loss between the heating cords and the center of the reaction volume. Unfortunately, the melting point of copper (*mp* = 1085 °C) was too low to accommodate the range of experimental conditions required. Choosing the correct material was a balancing act between a sufficiently large thermal conductivity and high enough melting point. Inconel 600, an alloy of nickel, chromium, and iron was eventually chosen as the material to house the heating wire Figure 28. This material has a melting point of 1673 K and range of thermal conductivity of 14.9 – 27.5 W/ m K for temperatures of 298 – 1073

Figure 28: Ridged Inconel body with grooves for heating elements

K respectively. Inconel 600 is oxidation-corrosion-resistant and well-suited for extreme pressure and heat. This material retains strength over a wide range of temperatures where materials like aluminum and steel would succumb to creep. While the structural properties of this material are perfect for this application the low thermal conductivity, compared to copper, raises a problem of heat loss from the heating wire to the center of the reaction volume. To accommodate this issue, the thickness of the Inconel in the grooves where the heating wire sits was made as thin as possible (1 mm) to reduce the distance between the heating wire and the reaction volume. The internal diameter of the Inconel tubing (r = 1.55 in.) was chosen to limit the distance, therefore heat loss, between the heating elements and the reaction volume. The whole Inconel block will still be heated to a uniform temperature and provide a homogenous heat source to the reaction volume. The pre-heating section also follow these design constraints. The heating wire used for this design are Thermocoax 2ZE|20/50-120/TI/CB20/KZ05/1m for the preheating section and Thermocoax 2ZE|30 G14.7%/50-120/TI/CB30/KZ05/1m for the main heating section Table 3. These are mineral insulated heating elements with a temperature range of up to +1000 °C. Because of the high temperatures encountered in the JSR experiments, it is imperative that the each heating cable have solid contact with the Inconel. Any portion of the heating cord that is not in direct contact with the Inconel could overheat and crack the insulation. If the insulation cracks the heating cords runs the risk of shorting out. This would lead to unforeseen cost and loss of time. To ensure that the heating cords are in sufficient contact with the Inconel, each will be vacuum-brazed into the grooves cut in the Inconel. Vacuum brazing employs vacuum so that the components undergoing the brazing will not react with excess oxygen, moisture,

Table 3: Design specifications for mineral insulated heating wire

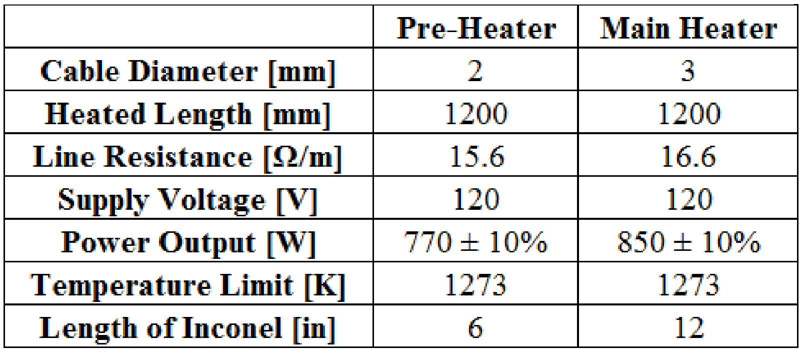

	Pre-Heater	Main Heater
Cable Diameter [mm]	2	3
Heated Length [mm]	1200	1200
Line Resistance [Ω/m]	15.6	16.6
Supply Voltage [V]	120	120
Power Output [W]	770 ± 10%	850 ± 10%
Temperature Limit [K]	1273	1273
Length of Inconel [in]	6	12

nitrogen, or other contaminants. By preventing reactions with the N_2/O_2 environment outside of the Inconel tubing, the filler alloy, a mixture of gold, copper and nickel, is able to flow easier onto metal surfaces and capillary joints. Using this method each heating cord will be completely surrounded by metal, reducing the risk of shorting out the cable. Each half of the main heating section will have 1200 mm of 3 mm diameter heating cable vacuumed brazed into the grooves. The groove pattern/ wrapping pattern was chosen to evenly spread the heat around the quartz reactor. Each preheating section will have 1200 mm of 2 mm diameter heating cable, while each main heating section will have similar length of 3 mm diameter heating cable. The larger diameter of the heating cords for the main heating section allows for higher resistance per meter and therefore higher temperatures. Along with the heating wires, mineral insulated K-type thermocouples will be vacuumed brazed into the Inconel grooves. These thermocouples will display the temperature of Inconel. Each of these heating wires, four in total, will be powered by a Variac voltage transformer. This will allow for precise control of the power output from the heating elements and temperature of the Inconel.

Ceramic Insulation

Insulation of the heating system has three equally important uses. The first is to prevent any heat from escaping to the surroundings. Any heat loss in the system will lower the maximum temperature achievable by this design. Secondly, the insulation is also used to reduce the dead volume inside the pressure vessel. This will reduce the amount of gas required to pressurize the reactor housing, and reduce the risk of injury in case of catastrophic failure. The third role of the insulation is user safety. Any material at these temperatures can cause serious injury when not properly handled. Thermal conductivity was the deciding factor when choosing a material for this. As opposed to the ridged body holding the heating elements, an extremely low thermal conductivity was needed to keep all of the heat directed towards the reaction volume. Accounting for all of these design parameters a thick ceramic insulation material was decided to be the best option due to its low thermal conductivity ($k = 0.346$ W/m·K) and its ridged, but easily machinable, structure. To maintain the ease of use the insulation is also separated into top and bottom halves that can be removed out of the top of the reactor Figure 29. For this application, Rescor 311 foam is used. This insulation is composed of alumina silica ceramic and withstands temperatures to 2000 K. It is resistant to oxidizing and reducing atmospheres, and will not out-gas in vacuum atmospheres. This material is easily machined to fit securely around the heating elements and reaction volume. A liquid hardener will be applied to the outer surface of the insulation to prevent dust and particles from breaking off and contaminating the inside of the reactor housing. The following calculations determine the thickness of insulation needed in order for the outer surface of

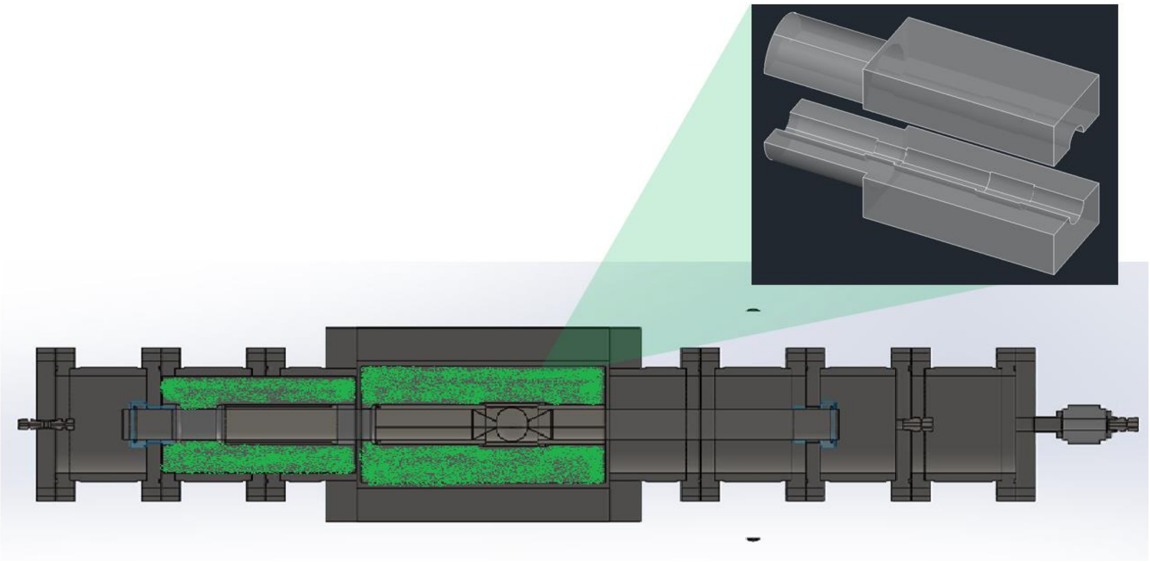

Figure 29: Location of the two halve of the ceramic insulation in relation to the reactor housing

the insulation to be room temperature when the heating elements are at their maximum temperature. Equation 8 is used to determine the heat transfer through a material in the radial direction.

$$T_2 - T_1 = -\frac{q}{2\pi kL} ln\frac{r_2}{r_1} \qquad 8$$

This equation can be rewritten to calculate the required thickness of the insulation. (Equation 9)

$$r_2 = r_1 * e^{\frac{2\pi kL\,(T_1 - T_2)}{q}} \qquad 9$$

Assuming the maximum temperature of the heating element (T_1 = 1273 K), room temperature on the outside of the ceramic insulation (T_2 = 300 K), the outer radius of the Inconel tubing (r_1 = .947”), length of the main heater (L = 12”), and all 850 W produced by the heaters is lost across the ceramic the required thickness can be calculated.

$$Required\,Thickness\ =\ r_2 - r_1 = 2.02\ \text{-}\ .947 = 1.073''$$

A thickness of 1 in. is needed in order to maintain outer surface at room temperature. The thickness of the insulation surrounding the pre-heaters is 1.5 in. and the minimum thickness of the insulation surrounding the main heater is 2in. This ensures that the outer surface will never reach above room temperature and not pose a safety concern.

Design of Two Pressure Volumes

Similar to temperature, many chemical reactions also have a strong dependence on the pressure. Higher pressures increase the number density and collision rate of the molecules during the reaction. This can have a variety of effects on the reaction including changes in ignition delay time, heat released, and most importantly products formed. The pressure inside the reaction volume is dependent on the flow rate, the composition of the fuel, oxidizer, and carrier gas entering the reactor, and the residence time of the gas inside the reaction volume. Specifics on how this is determined is outlined in the Experimental Details chapter (Section 5.2). As pressure builds inside the reaction volume eventually the structurally integrity of the quartz reaction would become compromised. To determine the pressure at which this might happen one can use the Young-Laplace equation (equation 10). σ is the hoop stress acting on the internal diameter of the quartz tubing in Pa, P is the internal pressure of the quartz tube in Pa, r in the internal radius of the tube in mm, and t is the wall thickness in mm.

$$\sigma = \frac{Pr}{t} \qquad 10$$

Properly annealed and de-stressed fused quartz can withstand up to 7000 kPa of internal hoop stress. With an internal radius of 17.3 mm and a wall thickness of 1.62 mm the quartz tube will be able to withstand up to 645 kPa or 6.37 atm of internal pressure. While this is sufficient for atmospheric and moderate pressure testing, this reactor is designed to conduct experiments at upwards of 50 atm. To reach pressures this high requires pressure balancing on the outside of the quartz tube Figure 30. This led to the stainless steel pressure vessel that surrounds the entirety of the quartz tube. As pressure increases inside the reaction volume a separate flow of nitrogen will pressurize the surrounding area to prevent the quartz from failing. As long as the pressure differential across the quartz remains below the 6.37 atm then the quartz will not fail. A simple pressure gage will monitor the pressure inside the reaction volume. The 4-20 mA signal from this gage will serve as the input for a Bronkhorst P-8x2CV pressure controller. The

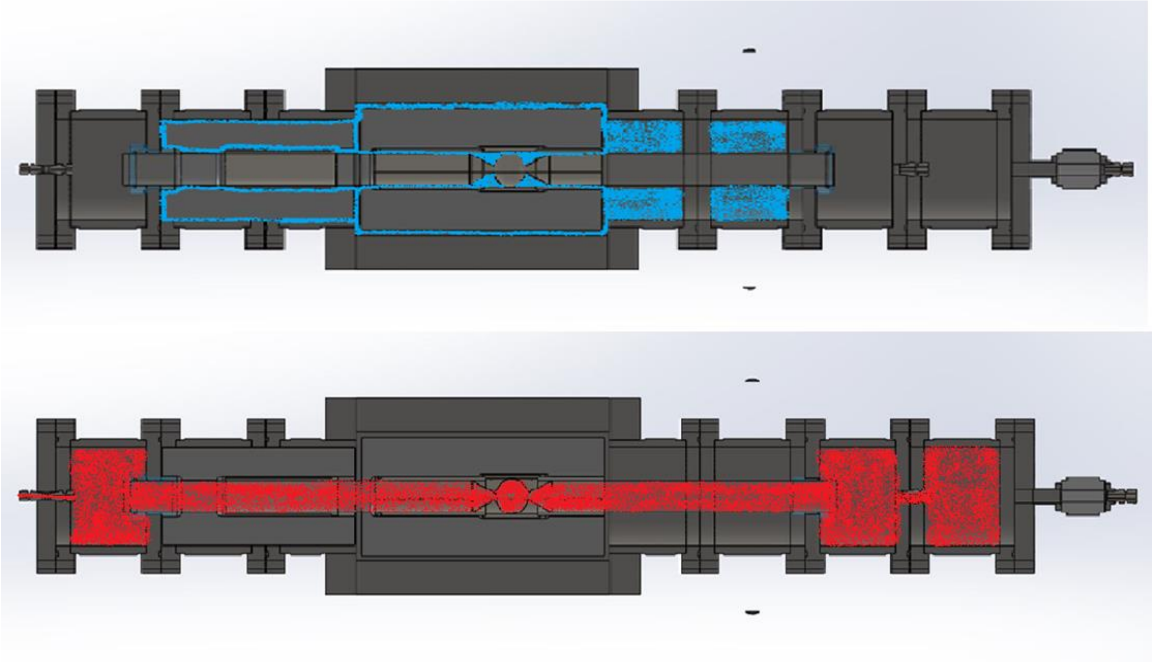

Figure 30: Red: Volume of reactant gases. Blue: Volume of balance gas. Pressure of these two volumes must be the same.

controller actively pressurizes and depressurizes the volume outside the quartz to match the pressure inside the reaction volume with an accuracy of ± 0.5% of its full-scale range of 200 atm. This is well within the range needed to prevent failure of the quartz. The use of this device will allow for static control of the pressure, which will prevent excess use of nitrogen.

In order to pressurize the reactor, the housing surrounding the reactor needs to be able to withstand the pressures in question. All sections are sealed with welds or pressure rated O-rings. All electrical feedthroughs are pressure rated compression fittings. All connectors are ¼ in. National Pipe Thread fittings which are designed for high-pressure applications. The square body in Section 3 is held together with bolts and an internal weld on all 90° corners. The bolts provide the structural support needed to withstand these high pressures and the weld provides an airtight seal. The lid is sealed with an O-ring and pressure rated bolts. Care should be taken when assembling this reactor. All O-rings should be properly secured in their groove before tightening down the bolts. All bolts should be tightened in a star pattern to apply even pressure on the O-rings. Failure to do so could lead to serious injury in case of catastrophic failure.

Von Mises stress analysis simulations were conducted in SolidWorks (Figure 31). This simulation shows the stress on the steel caused by internal pressures assuming all points inside see the same pressure, which is not the case in actual experiments where pressure relief is implemented in Sections 5 and 6. Two different simulations were conducted, one at 50 atm (750 psi) and one at 68 atm (1000 psi). For both pressures, the von Mises yield average is within the required amount for these internal pressures. This simulation provides evidence that the reactor housing not only meets the target pressure of 50 atm, but exceeds it by at least 18 additional atmospheres.

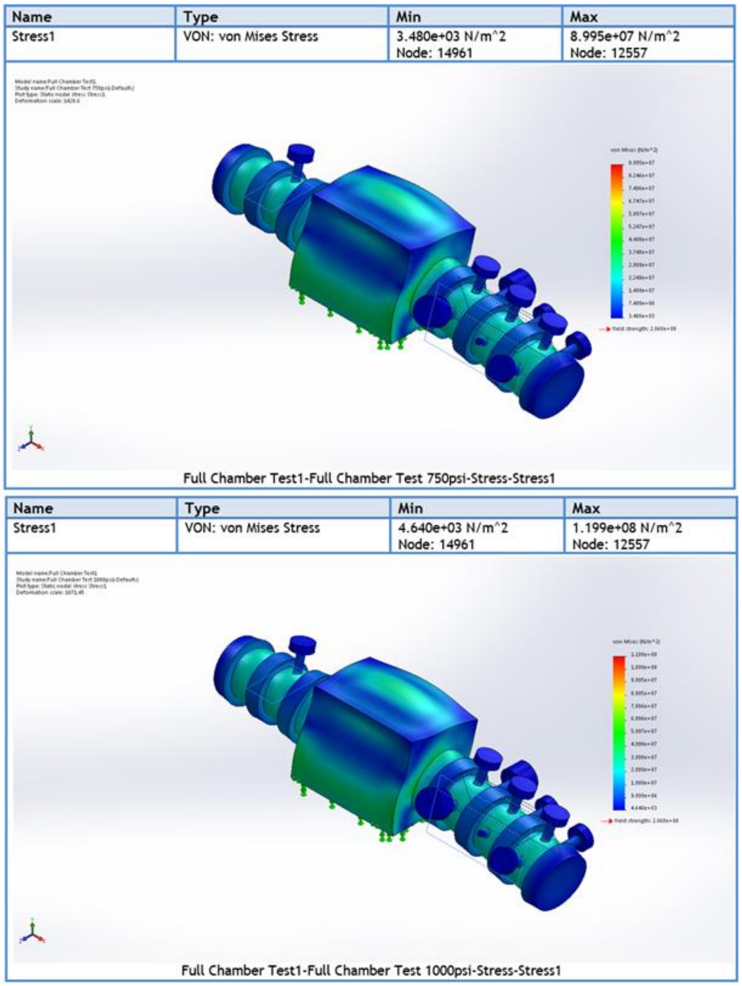

Name	Type	Min	Max
Stress1	VON: von Mises Stress	3.480e+03 N/m^2 Node: 14961	8.995e+07 N/m^2 Node: 12557

Full Chamber Test1-Full Chamber Test 750psi-Stress-Stress1

Name	Type	Min	Max
Stress1	VON: von Mises Stress	4.640e+03 N/m^2 Node: 14961	1.199e+08 N/m^2 Node: 12557

Full Chamber Test1-Full Chamber Test 1000psi-Stress-Stress1

Figure 31: Von Mises stress analysis simulations. Top: 50 atm (750 psi); Bottom: 68 atm (1000 psi)

Components of Post Reaction Pathways

After the fuel and oxygen have reacted inside the reaction volume for a given residence time, the products will flow through one of four paths (Figure 32). The first path will carry the bulk of the products through the exhaust port and into the waste stream. The second and third path flow through the sonic sampling probe. One path leads to collection of the products in specialized collection tanks. Details about the sonic

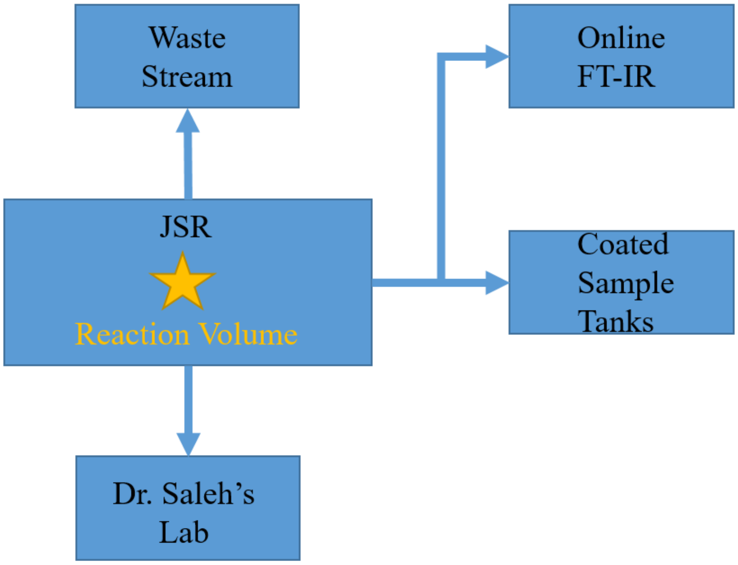

Figure 32: Post reaction pathways

sampling probe and collection tanks are located in the next section. The third path will direct the products to the FT-IR for analysis. The FT-IR will determine presence of CO, CO_2, and H_2O as a function of time. Reaction inside the reaction volume has reached steady state when the change in absorption signal from these molecules over a set amount of time has reached zero. The forth path will passively collect a small amount of the products and transport them to aerosol diagnostics in Professor Rawad Saleh's laboratory. Here, the products will undergo atmospheric aging to determine the potential effects these products will have on the atmosphere and environment. Professor Saleh focuses on secondary organic aerosols, SOAs, particle formation in the atmosphere, and the effects of brown and black carbon[32 33, 34] using a 7.5 m^3 atmospheric aging chamber, which produces UV light to simulate photo-oxidation caused by the sun. The amount of aging depends on the amount of oxidant present in the chamber. One hour in the chamber can be equivalent to one hour in the atmosphere, up to 12 hours. After reaction in this chamber the products are then analyzed with an array of analytical techniques. A

Scanning Mobility Particle Sizer (SMPS) measures aerosol size distributions between 10 nm and 1000 nm. The Aerosol Mass Analyzer coupled with Differential Mobility Analyzer (APM-DMA) measures the mass of size-selected aerosol particles. A Multi-PAS III photoacoustic instrument measures the light absorption by aerosol particles at three wavelengths (442, 532, 782 nm). This instruments determines the color of the particles and if they are classified as either brown carbon or black carbon. The coupling of Professor Rotavera's laboratory and Professor Saleh's laboratory will allow for unparalleled analysis of potential climate implications from increasing use of biofuels. With experiments constructed in this manor, these capabilities will be able to analyze the fundamental science and atmospheric impact of advanced combustion technologies. Professor Rotavera's capabilities will determine the composition and relative concentrations of the reaction products. This information will help determine a molecules potential use as a fuel or a fuel additive. Simultaneously, Professors Saleh's capabilities will determine the potential effects this molecule could have on the atmosphere and environment if it were to be used as a fuel or fuel additive.

Sonic Sampling Probe

Sonic sampling is a common technique[35, 36]. The sampling probe is a long probe made of fused quartz that is used to collect samples directly from the reaction volume and store them in collection tanks that are coated with intert material (Silconert). The probe design in the present work consists of 1/8 in. (diameter) x 33.5 in. (long) tube situated in the middle of a ¼ in. x 32 in. tube. At the tip, the 1/8 in. tube converges to an opening ranging from 100 - 500 μm in diameter, depending on the pressure conditions of interest. The 1/4 in. tube will converge around this opening sealing off the gap between the two tubes. A K-type thermocouple is installed down the length of the probe in the gap between the two tubes and sit in a well at the tip of the probe inside the ¼ in tube, but outside the 1/8 in tube (Figure 33). The tip of the thermocouple will be completely encased inside the probe to prevent any catalytic reactions taking place on the surface of the thermocouple tip. This thermocouple will measure the temperature of the gases in the reaction volume and therefore the temperature of the reactions. Temperature calibration is performed to account for any heat transfer effects that may be present between the wall thickness of the 1/8 in. quartz probe and the surface of the thermocouple. However, the magnitude of heat transfer is expected to be negligible given small surface area of the quartz.

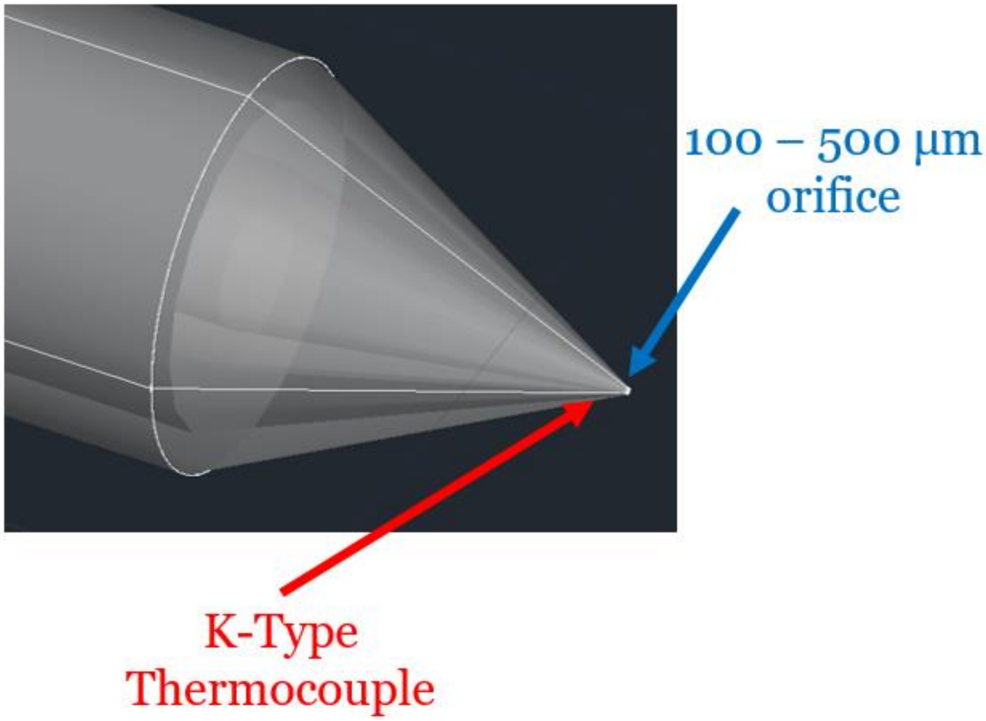

Figure 33: Tip of sonic sampling probe.

Due to the fragile nature of the material bracers have been placed along the length of the probe in between the 1/4” and 1/8” tubes to keep the 1/8” portion centered within the 1/4” portion, and to prevent a large moment arm from forming at the tip if any force is applied near the end. The ends of each tube were made different lengths in order to seal off the 1/4” section from the 1/8” section separately. These seals are 1/4” and 1/8” ultra-Torr fittings that have been built into the reactor housing.

Outside of the reactor housing, the ends of both tubes are connected to a Nor-Cal LMT-133 linear motion thimble (LMT). Because the LMT is designed for use in vacuum environments, proper precautions were taken to ensure the high pressures inside the reactor do not reach thimble. This thimble will allow the user to place the tip of the probe anywhere along the longitudinal axis of the reaction volume with accuracy on the order of 10 microns.

To sample from areas of the reaction volume outside the longitudinal axis a 45° probe can be used. A 45° probe is almost identical to a standard probe except the tip of the probe has been bent 45° to access the rest of the spherical volume. Utilizing the standard probe, 45° probe, and linear motion thimble allow the user to measure the temperature and collect samples from a large percentage of the reaction volume. This will be used to validate the assumption that are naturally present with this design. The assumption of uniform radial heating from the heating elements can be tested by measuring the temperature of the reaction gases at various points inside the reaction volume. A temperature gradient of less than 1 K inside the reaction volume is considered homogenous. The assumption of proper mixing from the jets can be tested by collecting samples from various positions in the reaction volume. If each of the samples have identical composition and species concentration then one can assume proper mixing is achieved by the jets. Without this validation of assumptions the results produced would have an error bar too large to be considered reliable data.

The sonic orifice located at the tip of the probe is made small enough to ensure the flow is sonic at the nozzle. The flow is sonic as long at the ratio between the pressure inside reaction volume and the pressure downstream exceeds the critical ratio given by equation 11[37], where γ is the specific heat ratio of the gas. Since the volume of carrier gas in the experiment is much larger than the volume of fuel and oxidant combined one can assume the gas in question is N_2 ($\gamma = 1.4$).

$$\frac{P_{rv}}{P_{ds}} \gg \left(\frac{\gamma + 1}{2}\right)^{\gamma/(\gamma-1)} \qquad 11$$

The mass flow rate through the probe can be calculated from equation 12, the mass balance equation applied to a sonic flow, where A is the cross sectional area of the sonic orifice, T is the temperature inside the reaction volume, and R is the gas constant for N_2 ($R = 296.8$ J/kg K).

$$\dot{m} = \frac{AP_{rv}}{\sqrt{T}} \sqrt{\frac{\gamma}{R}} \left(\frac{\gamma + 1}{2}\right)^{\frac{-(\gamma+1)}{2(\gamma-1)}} \qquad 12$$

The mass flow rate is primarily dependent on the area of the sonic orifice and the pressure inside the reaction area. To accommodate various flow rates and pressures, multiple probes were made with diameters of the sonic orifice ranging from 100 – 500 μm. This difference in pressure will allow for expansion cooling to occur as a sample is being collected effectively “freezing” a sample at time of collection. The term freezing is used to describe when the reactants are cooled from a temperature where reaction can spontaneously occur to a temperature well below that. The temperature at this point will still be above the dew point for the products formed.

Downstream of the linear motion thimble the 1/8” tube is connected to a sampling manifold that will dictate the path of the sample. One path includes a coated sample tank and a vacuum pump. The coating is an inert monolayer which lowers the potential of wall reactions inside the tanks. The tanks will be surrounded by heating jackets to prevent the sample from condensing inside of the tank. The vacuum pump will draw vacuum on the tank ensuring the tank is clean and free of any previous experiments. The flow rate to the pump, controlled by a valve, also dictates the pressure inside the sonic probe, P_{ds}. As long as the pressure inside the tank is low enough compared to the pressure inside the reaction volume to satisfy the conditions in equation 11 then the flow into the probe will be sonic. The second path included in the sampling manifold directs the reaction products towards the FT-IR for real time analysis.

CHAPTER 5

EXPERIMENTAL DESIGN

The reactor designed in the present work provides exceptional control over the experimental parameters described previously, namely temperature, pressure, residence time, and concentrations of gases. While these parameters are important for combustion related chemical kinetics, they are functions of other, more controllable, variables. In fact, the only points of control in these experiments are the voltage applied to the heating elements and the flow rates of the fuel, oxygen, and carrier gases. The section below describes how the flow of gas and voltage supply are manipulated in order to achieve the target experimental parameters.

Temperature Control

As discussed previously in Chapter 4, it is imperative that thermal homogeneity is achieved in the reaction volume for accurate chemical kinetics experiments. It terms of manipulating the temperature, there will be three areas of control that are regulated by five separate devices. The three areas are (1) the external pre-heater, (2) internal pre-heater, (3) and main heater. The internal pre-heater and main heater are each divided into two halves that are controlled by separate devices. For simplicity, and to satisfy the assumption of uniform radial heating, each half of these sections will be set to the same voltages at all times. The external pre-heaters serve the same purpose as the internal pre-heaters, to heat the gas gradually as it travels towards the reaction volume. This gradual heating insures that the entire volume of gas is heated and no cold spots, or thermal gradients, are present in the reaction volume. On the other hand, most hydrocarbons begin to thermally decompose around 500 K. This sets an upper limit for the target temperature in the pre-heating sections.

While the embedded thermocouples in each of the heating systems will communicate the actual temperature of each heating elements, the only point of control will the voltage supplied by a Variac transformer. The energy balance of a closed system can be applied to estimate the temperature of the heating elements when a certain voltage is applied for a determined amount of time (Equation 13). Assuming there is perfect contact between the heating cords and the Inconel tubing we can assume that there will be no loss of heat or energy between the two.

$$Q = mc_p(T_2 - T_1) \qquad 13$$

The power actually produced by the heating wires is a function of the voltage applied to it and the resistance of the heating wire (Equation 14).

$$Q = V^2/R \qquad 14$$

The line resistance is a material property that was set by the manufacture. 15.6 Ω/m for the internal pre-heater, and 16.6 Ω/m for the main heater. The variac transformer has the ability to provide voltages that range from 0 – 120 volts. The limiting factor is the voltage coming from the wall outlet in the lab. Retrofitting the lab with 240 V supply was discussed, but eventually decided against. Figure 34 shows an estimate of long it would take for one half of the main heating section to heat up when supplied with various voltages.

Figure 34 shows that the higher the voltage supplied to the heating cords the faster the Inconel tubing will heat. This is a major simplification that doesn't account for many real world problems including: heat loss through the material, heat loss to the ceramic insulation, and heat loss to the balance N_2 that will fill the dead volume. In reality, this curve will eventually level off as the heat supplied by the heating cords equals the heat lost to the surroundings. Similar analysis can be conducted for the internal and external pre-heating sections. Future validation testing is planned to determine the maximum temperature of the Inconel at the various voltages, but this plot provides an idea of what we expect to see. These validation tests will consist of applying a voltage to the heaters and measuring the temperature of the gases in reaction volume with thermocouple located in the sonic probe. This type of testing will yield the temperature of the gas at various flow rates for different voltages. Similar validation testing were completed for the external pre-heaters (Figure 35). An analogous plot will be developed for the internal pre-heater and the main heater. The goal of these plots are to have a guide that any user can

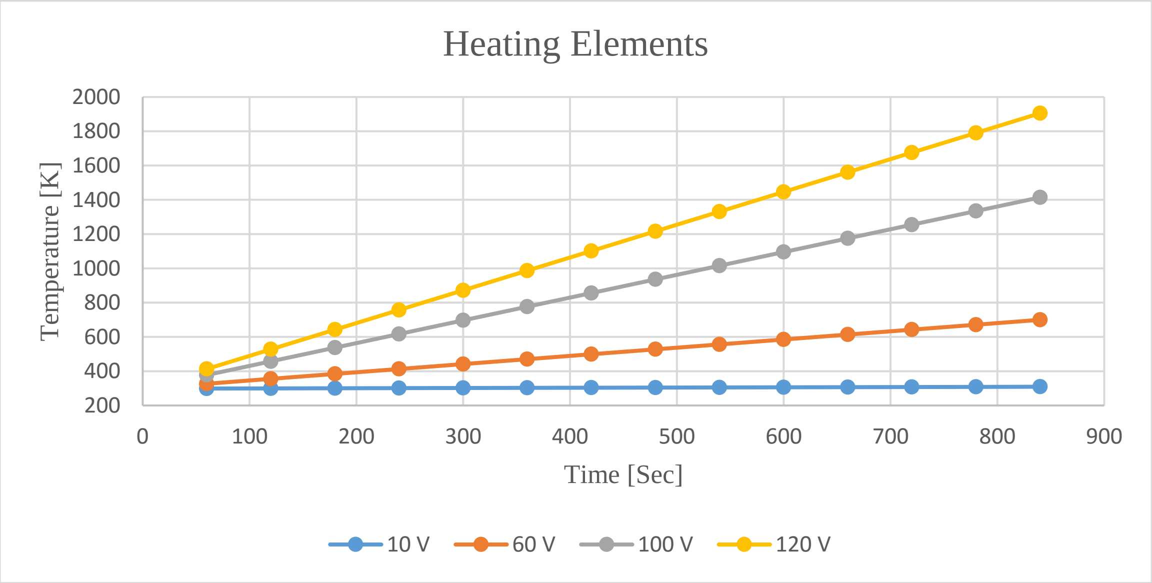

Figure 34: Time required to heat up one half of the main heating section at various voltages

reference when starting a new experiments. The voltages will need to be refined for each experiment depending on the composition of the gas, but this testing will provide a general idea of the temperature inside the reaction volume as a function of the flow rate through the reaction volume and the voltage applied to the heater. Eventually, tests will be conducted to determine the effect the pre-heaters have on the thermal homogeneity of the reaction volume. The end goal for these experiments is an empirically determined temperature correlation relating set temperature to actual temperature.

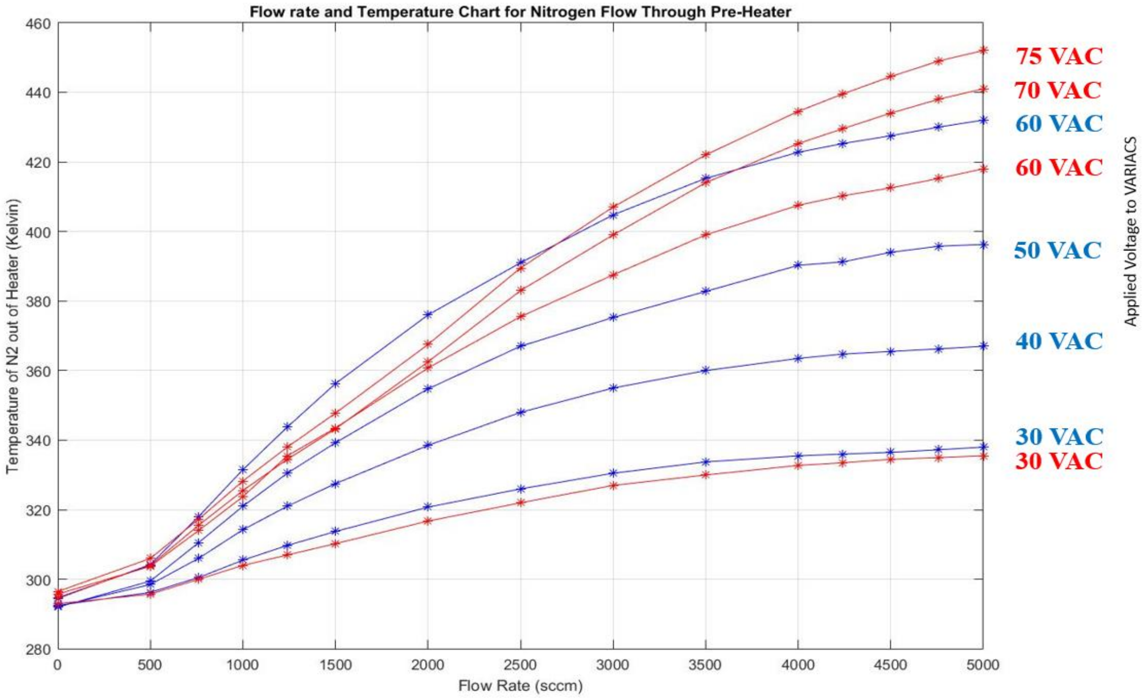

Figure 35: Temperature vs Flow Rate of N_2 through the external pre-heater for various voltages applied to the heater.

Control of the Flow Rates

The second point of control for this experiment is the flow of the various gases. This can be generalized into two separate flows, one for the fuel and one for the oxidizer. The liquid fuel will first be vaporized and mixed with N_2 as a carrier gas. The oxidizer, O_2, will also be mixed with a carrier gas before injection into the reactor. Nitrogen is used as a carrier gas to because of its inert properties. Also, since the mole fraction of N_2 is much greater than the mole fraction of O_2 or RH then the ideal gas assumptions can be applied to these experiments. The JSR conducts steady state experiments, meaning the conditions inside the reaction volume are not changing with time. One characteristic of steady state is the mass flow rate into the reactor equals the mass flow rate leaving the reactor (Equation 15). For this equation ρ is density, V is velocity of the gas, and A is the cross sectional area of the reactor.

$$(\rho VA)_{out} - (\rho VA)_{in} = 0 \qquad 15$$

Assuming ideal gas, flow the inlet flow conditions can be set equal to the conditions inside the reactor (Equation ID).

$$\left(\frac{P\dot{V}}{T}\right)_{Reactor} = \left(\frac{P\dot{V}}{T}\right)_{in} \qquad 16$$

Equation 16 can then be further simplified by using isentropic assumptions to develop an equation for the total volumetric flow rate of the gases through the reactor (Equation 17)

$$\dot{V}_{total} = \dot{V}\left({}^{T_o}/_{T}\right)\left({}^{P}/_{P_o}\right) \qquad 17$$

With the knowledge that the volumetric flow rate through the reaction volume can be expresses as the reaction volume divided by the residence time, an equation for the residence time can be determined (Equation 18).

$$\tau_{residence} = \left(\dot{V}_{total}/V_{reactor}\right)\left(T/T_o\right)\left(P_o/P\right) \tag{18}$$

The following plots show how the pressure, temperature, and residence time can be affected by altering the total flow rate through the reactor (Figures 36-38).

As mentioned above, the total flow rate is a combination of the flow of fuel/carrier gas and oxidizer/carrier gas. Specifically, the flow of the fuel/carrier gas, V_{vdm}, is a combination of the fuel flow rate, V_{RH}, and the flow rate of carrier gas, V_{RHC}. Similarly, the flow of the oxidizer/carrier gas, V_{ox}, is a combination of the oxidizer flow rate, V_{O2}, and the flow rate of carrier gas, V_{OC}. After the total flow rate is determines the V_{RH} and V_{O2} will need to be identified to satisfy the equivalence ratio required. The equivalence

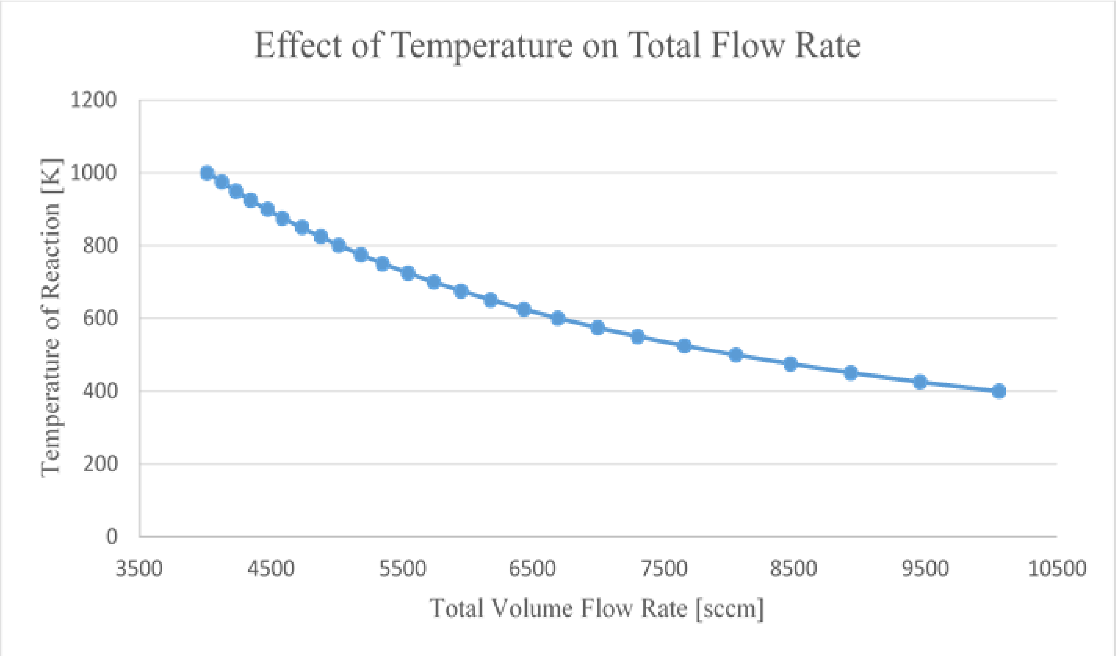

Figure 36: Effect of temperature on the total flow rate. Pressure and residence time were kept constant at 10 atm and 1.5 sec

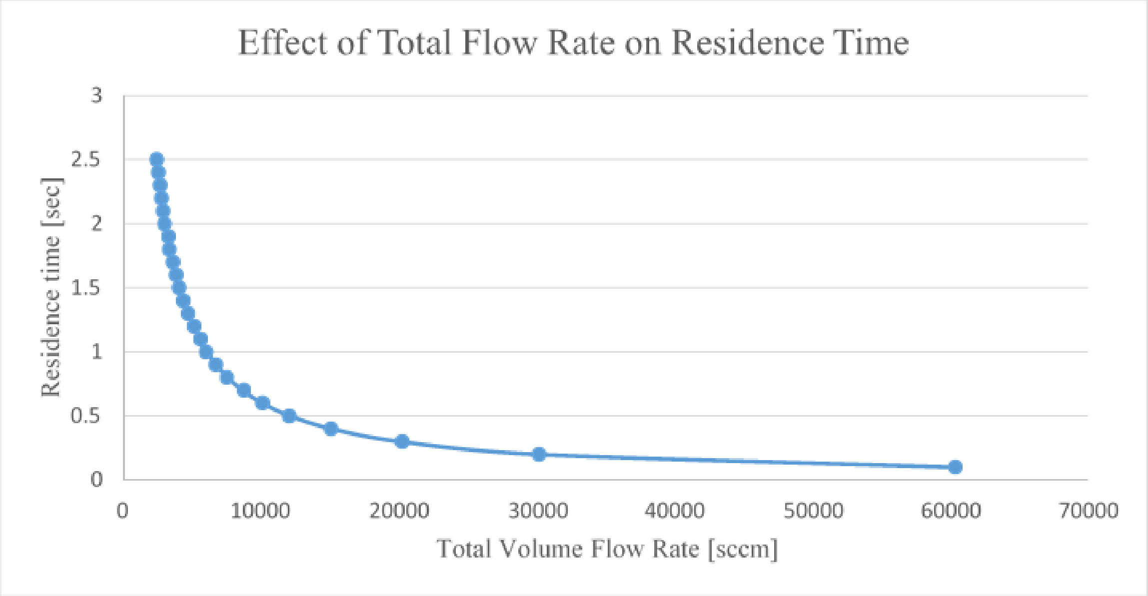

Figure 37: Effect of total volumetric flow rate on residence time. Pressure and temperature were kept constant at 10 atm and 1000 K

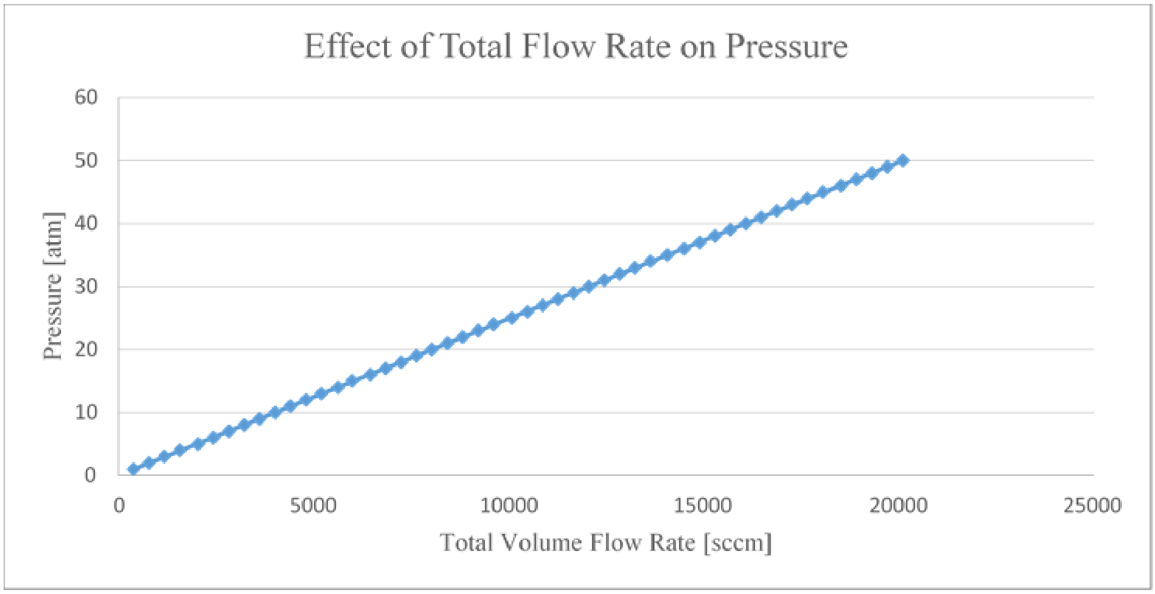

Figure 38: Effect of total volumetric flow rate on pressure. Residence time and temperature were kept constant at 1.5 s and 1000 K

ratio is the ratio of the actual fuel/oxidizer ratio to the stoichiometric fuel/oxidizer ratio (Equation 19). Stoichiometric ratio refers to ratio of fuel to oxidizer that, when completely combusted, will produce only carbon dioxide and water. This is considered ideal combustion because no energy is trapped in any unwanted products. The equivalence ratio determines if the fuel/oxidizer mixture is fuel lean, $\phi < 1$, or fuel rich, $\phi > 1$. This value can be manipulated to simulate the various concentrations of fuel and air inside a real world combustion system. If the mixture is fuel-lean the reaction products are more likely to contain excess oxygen. On the other hand, if the mixture is fuel rich the reaction products are more likely to contain extra carbon molecules. As the equivalence ratio moves further away from stoichiometric the probability of the formation of unwanted reaction products increases. This only adds to the already complex chemistry that is characteristic of low temperature combustion. Precise control of the equivalence ratio is therefore imperative to ensure accurate initial conditions.

$$\Phi = \frac{\left(\bar{N}_{RH}/\bar{N}_{O_2}\right)}{\left(\bar{N}_{RH}/\bar{N}_{O_2}\right)_{stoich}} \qquad 19$$

The concentration of fuel is predetermined by the experimental goals and is usually kept constant in a given series of measurements. Since combustion reactions are exothermic, fuel concentration in the JSR experiments is minimized to ensure that heat release during combustion does not alter the temperature of the reaction volume, which maintains isothermal conditions. For experiments conducted in this reactor the fuel concentrations will be kept at 1000 ppm while the oxidizer concentration will fluctuate to satisfy various equivalence ratios and oxygen concentrations of interest. With the concentration of the fuel predetermined, the volumetric flow rate of the fuel can be calculated using Amagat's Law, equation 20.

$$\dot{V}_{RH} = y_{RH}\dot{V}_{total} \qquad 20$$

With the volumetric flow rate of the fuel determined, the flow rate of the oxidizer can be found by rearranging equation 19. Ideal gas and Amagat's Law assumptions allow the molar concentrations in equation 19 to be substituted with volumetric flow rates to form Equation 21. This equation takes into account the volumetric flow rate of the fuel and the equivalence ratio to determine the required flow rate of the oxygen.

$$\dot{V}_{O_2} = \frac{\Phi^{-1}\dot{V}_{RH}}{\left(\dot{V}_{RH}/\dot{V}_{O_2}\right)_{Stoich}} \qquad 21$$

With the flow rate of the fuel and oxygen known, the flow rate of both carrier gases is set so the sum of all four flow rates equals the total flow rate required. To do this, a dilution factor for the fuel must be chosen. This dilution factor (*df*) is an arbitrary value that depends on the volatility of the fuel being studied and is needed to determine the level of dilution in the flow rate V_{vdm}. For example, a dilution factor of 0.9 means that V_{vdm} will consist of 90% N_2 and 10% fuel (RH). Therefore, the flow rate of the fuel carrier gas, V_{RHC}, can be determined by Equation 22. This only leaves the flow rate of the oxidizer carrier gas to be fixed. This is done by summing the known volumetric flow rates and subtracting them from the total flow rate (equation 23).

$$\dot{V}_{RHC} = \dot{V}_{RH} \Big/ (1 - df\,) \qquad 22$$

$$\dot{V}_{OC} = \dot{V}_{total} - \left(\dot{V}_{RH} + \dot{V}_{RHC} + \dot{V}_{O_2}\right) \qquad 23$$

By controlling the flow rates of the gases and the temperature of the reaction volume a wide range of experimental conditions can be achieved. While determining the required flow rates can get quite complex, especially when conducting multiple experiments in a short amount of time, spreadsheets were developed to conduct flow rate calculations.

CHAPTER 6

FUTURE WORK AND CONCLUSIONS

A high pressure jet-stirred reactor was designed and built for gas phase chemical kinetics measurements. While thorough preparation went into the design of each part of the reactor, validation testing is still required to determine the accuracy of the experiments. This includes isolated testing of the following sections:

- Temperature correlation experiments in pre-heating and main heating regions
- Pressure balancing/regulation system testing
- Sampling system testing
- Thermal homogeneity measurements of reaction volume

Once the individual sections have been tested, the first fuels in line to be tested are a family of C_4 molecules including: n-butane, 1-butanol, butanone, tetrahydrofuran, and diethyl ether. These fuels are ideal for testing the capabilities of the reactor and facilitating components because the short carbon chains limit the number of potential reaction products. Also, experimental data for these fuels conducted at similar conditions in a different experimental device are available for comparison. Once the reactor yields similar results to previous studies then more complex fuels can be studied.

In 2007 the United States passes the Energy Independence and Security Act. This act states that the U.S. will strive to increase the production of clean renewable fuels and increase the efficiency of vehicles and products using these fuels in order to reduce the United States' dependence on petroleum bases fuels. This act will have numerous positive effects for the environment and economy of the U.S. Integration of these fuels into the transportation sector will reduce climate change across the world by reducing the net release of greenhouse gases into the atmosphere. Securing a biomass and fuel source on domestic soil will reduce the volatility of fuel prices and secure the United States' position as a leader in science and technology, which has been a long time standard for economic success. This will also create jobs in the agriculture, bio-science, and transportation fields. Low temperature – high pressure combustion of renewable fuels is a means of integrating this act into the transportation sector. Combusting fuels at low temperatures has proven to reduce the production of harmful pollutants. This idea of cleaner burning combustion has been coupled with high pressure engine design to produce high efficiency and lower emission engines. In order to maximize the benefits from low temperature – high pressure combustion experimental data of potential renewable fuels is needed. The current combustion models would benefit from experimental data in these temperature and pressure ranges to more accurately model the combustion process. More accurate combustion models will allow for engine designers to build more precise and efficient engines.

The core design of quartz reactor is based off previous JSR designs pioneered by Dagaut et al[22]. The novelty of the present design comes from its ability to reach experimental conditions that, until now, have been inaccessible for comparable reactors. The innovative heating design eliminates cold spots and thermal gradients and insures a homogenous temperature inside the reaction volume. The pressure vessel encapsulating the reactor and pressure balancing system allows for experiments to be conducted at pressures up to 50 atm. The state of the art analytical techniques facilitating this reactor will provide isomeric resolution and concentrations of the reaction products. The results from conducting experiments at this facility will fill the gap in experimental data for low temperature – high pressure combustion reactions.

REFERENCES

[1] Herbinet, O., and Dayma, G. (2013) Jet-Stirred Reactors, In *Cleaner Combustion: Developing Detailed Chemical Kinetic Models* (Battin-Leclerc, F., Simmie, J. M., and Blurock, E., Eds.), pp 183-210, Springer London, London.

[2] Zádor, J., Fernandes, R. X., and Taatjes, C. A. (2011) Kinetics of elementary reactions in low-temperature autoignition chemistry, *Progress in Energy and Combustion Science 37*, 371-421.

[3] Administration, U. S. E. I. (2017) Annual Energy Outlook 2017.

[4] Rotavera, B., Savee, J. D., Antonov, I. O., Caravan, R. L., Sheps, L., Osborn, D. L., Zádor, J., and Taatjes, C. A. (2017) Influence of oxygenation in cyclic hydrocarbons on chain-termination reactions from R+ O2: tetrahydropyran and cyclohexane, *Proceedings of the Combustion Institute 36*, 597-606.

[5] Buda, F., Bounaceur, R., Warth, V., Glaude, P.-A., Fournet, R., and Battin-Leclerc, F. (2005) Progress toward a unified detailed kinetic model for the autoignition of alkanes from C4 to C10 between 600 and 1200 K, *Combustion and flame 142*, 170-186.

[6] Metcalfe, W. K., Burke, S. M., Ahmed, S. S., and Curran, H. J. (2013) A hierarchical and comparative kinetic modeling study of C1− C2 hydrocarbon and oxygenated fuels, *International Journal of Chemical Kinetics 45*, 638-675.

[7] Fisher, E. M., Pitz, W. J., Curran, H. J., and Westbrook, C. K. (2000) Detailed chemical kinetic mechanisms for combustion of oxygenated fuels, *Proceedings of the combustion institute 28*, 1579-1586.

[8] Basevich, V. Y., Belyaev, A., Posvyanskii, V., and Frolov, S. (2013) Mechanisms of the oxidation and combustion of normal paraffin hydrocarbons: Transition from C 1–C 10 to C 11–C 16, *Russian Journal of Physical Chemistry B 7*, 161-169.

[9] Harper, M. R., Van Geem, K. M., Pyl, S. P., Marin, G. B., and Green, W. H. (2011) Comprehensive reaction mechanism for n-butanol pyrolysis and combustion, *Combustion and Flame 158*, 16-41.

[10] Battin-Leclerc, F., Simmie, J. M., and Blurock, E., (Eds.) (2013) *Cleaner Combustion*, Springer-Verlag, London.

[11] Burke, S. M., Metcalfe, W., Herbinet, O., Battin-Leclerc, F., Haas, F. M., Santner, J., Dryer, F. L., and Curran, H. J. (2014) An experimental and modeling study of propene oxidation. Part 1: Speciation measurements in jet-stirred and flow reactors, *Combustion and Flame 161*, 2765-2784.

[12] Koritzke, A. L., Davis, J. C., Caravan, R. L., Christianson, M. G., Osborn, D. L., Taatjes, C. A., and Rotavera, B. (2018)˙ QOOH-mediated reactions in cyclohexene oxidation, *Proceedings of the Combustion Institute*.

[13] Koritzke, A. L., Davis, J. C., Caravan, R. L., Christianson, M. G., Osborn, D. L., Taatjes, C. A., and Rotavera, B. (2019)˙ QOOH-mediated reactions in cyclohexene oxidation, *Proceedings of the Combustion Institute 37*, 323-335.

[14] Lai, J. Y. W., Lin, K. C., and Violi, A. (2011) Biodiesel combustion: Advances in chemical kinetic modeling, *Progress in Energy and Combustion Science 37*, 1-14.

[15] David, R., and Matras, D. (1975) Règies de construction et d'extrapolation des réacteurs auto-agités par jets gazeux, *The Canadian Journal of Chemical Engineering 53*, 297-300.

[16] Azay, P., and Côme, G.-M. (1979) Temperature gradients in a continuous flow stirred tank reactor, *Industrial & Engineering Chemistry Process Design and Development 18*, 754-756.

[17] Zhao, H. (2007) *HCCI and CAI engines for the automotive industry*, Elsevier.

[18] Razus, D., Movileanu, C., Brinzea, V., and Oancea, D. (2007) Closed vessel combustion of propylene–air mixtures in the presence of exhaust gas, *Fuel 86*, 1865-1872.

[19] Vasu, S. S., Davidson, D. F., and Hanson, R. K. (2008) Jet fuel ignition delay times: Shock tube experiments over wide conditions and surrogate model predictions, *Combustion and flame 152*, 125-143.

[20] Miller, J. A., Mitchell, R. E., Smooke, M. D., and Kee, R. J. (1982) Toward a comprehensive chemical kinetic mechanism for the oxidation of acetylene: comparison of model predictions with results from flame and shock tube experiments, In *Symposium (International) on Combustion*, pp 181-196, Elsevier.

[21] Egolfopoulos, F. N., Hansen, N., Ju, Y., Kohse-Höinghaus, K., Law, C. K., and Qi, F. (2014) Advances and challenges in laminar flame experiments and implications for combustion chemistry, *Progress in Energy and Combustion Science 43*, 36-67.

[22] Dagaut, P., Cathonnet, M., Rouan, J., Foulatier, R., Quilgars, A., Boettner, J., Gaillard, F., and James, H. (1986) A jet-stirred reactor for kinetic studies of homogeneous gas-phase reactions at pressures up to ten atmospheres (≈ 1 MPa), *Journal of Physics E: Scientific Instruments 19*, 207.

[23] Marquaire, P. M., and Come, G. M. (1978) Non Quasi-Stationary State Pyrolysis Induction Period of Neopentane Pyrolysis, *React Kinet Catal L 9*, 165-169.

[24] Herbinet, O., Marquaire, P.-M., Battin-Leclerc, F., and Fournet, R. (2007) Thermal decomposition of n-dodecane: Experiments and kinetic modeling, *Journal of analytical and applied pyrolysis 78*, 419-429.

[25] Dagaut, P., Boettner, J.-C., and Cathonnet, M. (1996) Chemical kinetic study of dimethylether oxidation in a jet stirred reactor from 1 to 10 ATM: Experiments and kinetic modeling, *Symposium (International) on Combustion 26*, 627-632.

[26] Dagaut, P., Reuillon, M., Boettner, J.-C., and Cathonnet, M. (1994) Kerosene combustion at pressures up to 40 atm: Experimental study and detailed chemical kinetic modeling, *Symposium (International) on Combustion 25*, 919-926.

[27] Baulch, D., Griffiths, J., Pappin, A. J., and Sykes, A. F. (1988) Stationary-state and oscillatory combustion of hydrogen in a well-stirred flow reactor, *Combustion and flame 73*, 163-185.

[28] Rousso, A. C., Hansen, N., Jasper, A. W., and Ju, Y. (2018) Low-Temperature Oxidation of Ethylene by Ozone in a Jet-Stirred Reactor, *The Journal of Physical Chemistry A 122*, 8674-8685.

[29] Battin-Leclerc, F., Herbinet, O., Glaude, P. A., Fournet, R., Zhou, Z., Deng, L., Guo, H., Xie, M., and Qi, F. (2010) Experimental confirmation of the low-temperature oxidation scheme of alkanes, *Angewandte Chemie International Edition 49*, 3169-3172.

[30] Pilling, M. J. (1997) *Low-temperature combustion and autoignition*, Vol. 35, Elsevier.

[31] Serinyel, Z., Lailliau, M., Thion, S., Dayma, G., and Dagaut, P. (2018) An experimental chemical kinetic study of the oxidation of diethyl ether in a jet-stirred reactor and comprehensive modeling, *Combustion and Flame 193*, 453-462.

[32] Saleh, R., Robinson, E. S., Tkacik, D. S., Ahern, A. T., Liu, S., Aiken, A. C., Sullivan, R. C., Presto, A. A., Dubey, M. K., and Yokelson, R. J. (2014) Brownness of organics in aerosols from biomass burning linked to their black carbon content, *Nature geoscience 7*, 647.

[33] Saleh, R., Hennigan, C., McMeeking, G., Chuang, W., Robinson, E., Coe, H., Donahue, N., and Robinson, A. (2013) Absorptivity of brown carbon in fresh and photo-chemically aged biomass-burning emissions, *Atmospheric Chemistry and Physics 13*, 7683-7693.

[34] Saleh, R., Cheng, Z., and Atwi, K. (2018) The brown–black continuum of light-absorbing combustion aerosols, *Environmental Science & Technology Letters 5*, 508-513.

[35] Sarathy, S. M., Thomson, M. J., Togbé, C., Dagaut, P., Halter, F., and Mounaim-Rousselle, C. (2009) An experimental and kinetic modeling study of n-butanol combustion, *Combustion and Flame 156*, 852-864.

[36] Gaïl, S., Thomson, M. J., Sarathy, S. M., Syed, S. A., Dagaut, P., Diévart, P., Marchese, A. J., and Dryer, F. L. (2007) A wide-ranging kinetic modeling study of methyl butanoate combustion, *Proceedings of the Combustion Institute 31*, 305-311.

[37] Maroteaux, D., Maroteaux, F., and Murat, M. (1991) Experimental study of a hot wire, sonic nozzle probe for concentration measurements, *Review of scientific instruments 62*, 1057-1062.